Numerical Investigation of Pattern Dynamics in Complex Ginzburg-Landau Equation

A Thesis
Submitted for the Degree of
Master of Science (Engineering)
in the Faculty of Science

by

Saugata Patra

Theoretical Sciences Unit
Jawaharlal Nehru Centre for Advanced Scientific Research
Bangalore – 560 064

FEBRUARY 2013

Dedicated to my family

DECLARATION

I hereby declare that the matter embodied in the thesis entitled "**Numerical Investigation of Pattern Dynamics in Complex Ginzburg-Landau Equation**" is the result of investigations carried out by me at the Theoretical Sciences Unit, Jawaharlal Nehru Centre for Advanced Scientific Research, Bangalore, India under the supervision of Dr. Subir K Das and that it has not been submitted elsewhere for the award of any degree or diploma.

In keeping with the general practice in reporting scientific observations, due acknowledgement has been made whenever the work described is based on the findings of other investigators.

Saugata Patra

CERTIFICATE

I hereby certify that the matter embodied in this thesis entitled "**Numerical Investigation of Pattern Dynamics in Complex Ginzburg-Landau Equation**" has been carried out by Ms. Saugata Patra at the Theoretical Sciences Unit, Jawaharlal Nehru Centre for Advanced Scientific Research, Bangalore, India under my supervision and that it has not been submitted elsewhere for the award of any degree or diploma.

Dr. Subir K Das
(Research Supervisor)

Acknowledgement

I hereby express my sincere gratitude to my research supervisor Dr. Subir K Das for his guidance throughout my work.

I also express my hearty thanks to all my labmates Suman, Sutapa, Subhajit, Jiarul and Saikat for their help and useful discussions.

I am also grateful to Prof. Umesh V. Waghmare, Prof. Srikanth Sastry, Prof. Sobhana Narasimhan, Prof. Kavita Jain, Prof. Swapan K Pati, Prof. N. S. Vidhyadhiraja and Prof. Balasubramanian Sundaram for what I have learned from the courses offered by them.

I also express my thanks to all my friends in JNC for making my life enjoyable here.

Most of all I am thankful to my family for their love and constant support throughout my life.

Synopsis

Beautiful patterns are very common in nature. Often similar patterns are observed in many different systems and in varied length scales. There has been significant recent activities in understanding pattern formation and underlying universality. In the theoretical literature of pattern formation, among others, the complex Ginzburg-Landau (CGL) equation, written as

$$\frac{\partial\psi(\vec{r},t)}{\partial t} = \psi(\vec{r},t)+(1+i\alpha)\nabla^2\psi(\vec{r},t)-(1+i\beta)|\psi(\vec{r},t)|^2\psi(\vec{r},t), \tag{1}$$

has received much attention. In Eq.(1), ψ is a space- and time-dependent complex order parameter, while α and β are real parameters. This equation has very diverse applications, encompassing physics, chemistry and biology. In chemistry, e.g., the CGL equation can be used to understand spiral pattern in Belouzov-Zhabotansky (BZ) reaction, since, for large ranges of the parameter values α and β, CGL equation exhibits spiral dynamics. In this thesis, we have been interested in numerically studying pattern formation and related dynamics in the CGL equation.

In the **Introductory chapter** of the thesis we discuss the basics of pattern formation. There the CGL equation is introduced in significant length. In addition, we also present various analytical and numerical tools to understand pattern formation.

In the limiting case $\alpha = \beta = 0$, Eq. (1) becomes the real Ginzburg-Landau (RGL) equation where the pattern is characterized by vortex defect, a special case of spiral. Here we note that, the multi-spiral patterns are frozen in the CGL equation which is not the case for RGL. From the single defect solution of the CGL equation, obtained by P.S. Hagan and others, it appears that, rather generally, for $\alpha = \beta = \lambda$, the defect structure is vortex. So, it is of obvious interest to make a general study for $\alpha = \beta$, in the multi-defect context. In the **second chapter**, we present results from comparative studies of CGL equation for wide range of values of λ. Interestingly, we observe that the pattern and dynamics, in general, for $\alpha = \beta$, are quantitatively similar to the RGL equation. Here, we note that, even though single spiral solution generally predicts vortex structure for $\alpha = \beta$, the frequencies of the traveling wave solutions, which is zero for RGL, are different. So, it is not very straight forward to anticipate that the inter-defect interaction is same for all values of $\alpha = \beta$. Nevertheless, our quantitative results, presented in this chapter, for the pattern and dynamics, is suggestive of that and supports some approximate analytical calculations. This observation also verifies the utility of single-defect solution in multi-defect context. In addition, we presented results from single-spiral experiments as well, to verify some other crucial aspects of Hagan's solution.

In **third and the last chapter**, we present results on the effects of disorder in α and β in the otherwise frozen spiral dynamics when $\alpha \neq \beta$. Note that in the context of BZ reaction, α and β are interpreted as the catalyst concentration and diffusivity, which are never constant in space. A recent study was motivated by this later fact where effect of disorder in β (by fixing $\alpha = 0$) was found to be positive in unlocking the frozen dynamics. In this chapter, we show that disorder in both α and β can unlock the frozen spiral dynamics in CGL equation.

Contents

List of Figures

Chapter 1

Introduction

Interesting patterns are observed almost everywhere in nature starting from structure of a cell to that of a galaxy. In the area of pattern formation [1], an interesting fact is that similar patterns are observed in a vast variety of systems, giving rise to universalities. There is strong recent research interest [2–10] in finding explanation of the appearance and further evolution of various types of patterns and selection of one pattern over the other. In addition to natural science, it will have applications in many other fields, e.g., economics, population dynamics, etc [11]. A primary aim of studies on pattern formations [1] is to identify the similarities in patterns in apparently different systems and to develop theories for a quantitative understanding for this important and interesting universal phenomena.

1.1 Universality of patterns

Examples of some patterns are shown in Figs.1.1 and 1.2. In Fig.1.1, it is interestingly observed that striped patterns are present in a wide variety of systems like sand ripples in desert, black and white stripes on zebra skin, black stripes on tiger skin, pattern on wood. In these examples, although the systems are very different in nature and size, they exhibit such striking similarity in structure. Similarly in Fig.1.2, it is observed that the beautiful spiral patterns are present in diverse systems in nature like galaxy, structure of broccoli, spiral arrangement of florets in sunflower and spiral pattern in sea-snail. Further description and in some cases mechanisms (if understood), taking help of Wikipedia and other references [1, 12], responsible to form some of these patterns are given in brief below.

The reason for the sand ripple formation in desert is the action of wind on loose sand. For strong enough wind, the sand-grains are lifted by the air and carried to some distance. Then due to the weight they are unable to stay suspended for long time, so return to the ground again. While returning they impart significant energy and momentum to the ground sand and energize other grains to fly. These later grains have lower energy because of which they can fly up only a small distance. This generates a cascade process. There exist many models [13–23] to explain the emergence of ripples under discussion. One of these is the

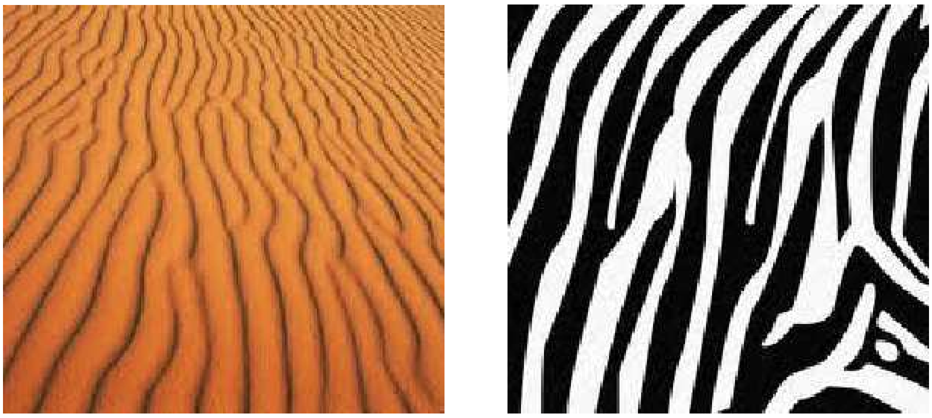

(a) Ripples of sand in desert (b) Zebra skin

(c) Tiger skin (d) Pattern on wood

Figure 1.1: Some striped patterns observed in different objects in nature are shown. (a) Sand ripples formed due to the action of wind. (b) Striped patterns on zebra. (c) Pattern on tiger's skin. (d) The striped pattern observed on wood. Source: bbpaperandink.com, amstranger.blogspot.com, art.com, ukflooringdirect.co.uk

(a) Spiral galaxy (b) Romanesco broccoli

(c) Sunflower (d) Sea snail

Figure 1.2: Some beautiful spiral patterns observed in nature are shown. (a) Spiral galaxy. (b) A small portion of broccoli (Italian cauliflower). (c) The spiral arrangement of florets in sunflower. (d) The spiral pattern of cleavage on the shell of a sea snail. Source: nasa.gov, leavingbabylon.wordpress.com, wikipedia.org, elephantjournal.com

Anderson model [22, 23]. Understanding from this model states that the ripple formation occurs entirely due to the spatial variation of the flux of these low energy grains.

The patterns on animal skin is due to morphogenesis [11] which essentially is a chemical reaction involving substances called the morphogenes along with the diffusion through the tissue. Such a system, originally being quite homogeneous, may later develop a pattern or structure due to an instability set by some perturbation.

A galaxy consists of stars and other interstellar objects. It has a spiral structure. There the spiral arms may form due to some disturbance in a uniformly rotating mass of stars. These spiral arms are the areas of high-density matters. Due to high gravitational pull in the spiral arm regions, the stars accumulate in these regions and thus resulting in the growth of the spirals.

Romanesco broccoli resembles a cauliflower but green in colour. It has a self-similar structure where the branched meristem (the tissue in plants which makes the leaves, flowers, etc.) makes the so called logarithmic spirals. Each bud there is composed of a series of similar smaller buds all of which are again arranged in a similar logarithmic spirals. This self-similar structure continues to several smaller levels.

In Fig.1.2, we also show sunflower which consists of numerous florets. (The florets inside the circular head mature into seeds.) The florets arrange themselves in interconnecting logarithmic spirals in order to gain the closest packing structure.

In Fig.1.3 we show further interesting spiral pattern in colonies of the slime mold Dictyostelium discoidium amoeba. When deprived of heat or moisture, members of the colony start cross-talk. This communication helps them aggregate into multicellular bodies that can better survive hardship. Essentially depending upon the need some pioneer cells release pulse of the compound called cyclic adenosine monophosphate (cAMP) and nearby cells then follow this trail. When a slime mold colony starts to undergo such chemotaxis, it behaves as an excitable medium and forms spiral structure involving the moving cells.

Our last example of spiral structure here is from the Belousov-Zhabotansky reaction [24] shown in Fig.1.4. This is an oscillatory chemical reaction. In this reaction, malonic acid is oxidized by bromate ions in presence of cerium catalyst. During the process, cerium breaks into Ce(III) ions which is colorless and Ce(IV) ions which is yellow in colour. These two different ions arrange themselves in such a way that some white spirals are seen in yellow background. Basically, the fixed concentrations of Ce(III) form spiral.

So, it was quite clear that similar patterns can form in very different systems. Even though mechanisms for similar patterns in different systems may appear different, it should still be possible to bind them under same theoretical framework. As already mentioned, an objective in the area of nonequilibrium statistical mechanics is to gain understanding of

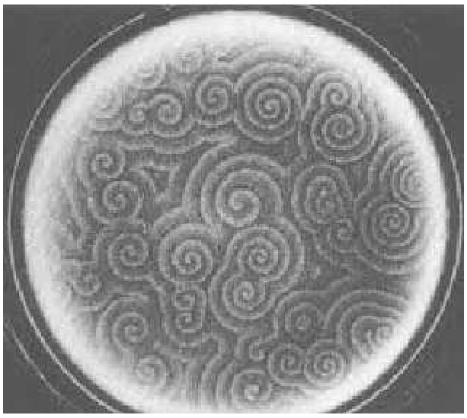

Figure 1.3: Slime-mold colony of Dictyostelium-Discoidium amoeba. The bright regions correspond to the accumulation of moving cells, forming spiral structures. Source: metafysica.nl

Figure 1.4: Spiral patterns in Belousov-Zhabotansky reaction. Some white spirals are observed in the yellow background which are due to variation of concentration of ions of some chemical species. Source: sciencephoto.com

such pattern formation under unified framework. Here we also note that many interesting and beautiful patterns are due to presence of defects [25] that destroy the regular ordering of the relevant order-parameter. Below we discuss some important defect structures.

1.2 Topological defects

A defect can be defined as point, line, or surface where the order parameter vanishes. Thus we need here to define the order parameter. An order parameter is the quantity which characterizes the ordering of the system and useful in the context of phase transition. E.g., in magnetic systems magnetization is zero above the critical or Curie point when the system is completely disordered (paramagnetic phase) and is non-zero below the critical point when the system is partially or completely ordered (ferromagnetic phase). So the quantity “magnetization” is the order parameter in ferromagnetic systems. One of the simplest defects is the domain wall in multi-component mixtures where domains of different species are separated from each other by the wall. Typically, in this case the order-parameter is a scalar quantity. In general for d-dimensional system, with n-component vector order parameter, the defect is (d-n)-dimensional [25]. E.g., in 2-dimensional system with scalar order parameter(i.e, n=1), the defects are the line boundary (i.e, 1-dimensional), in 2-dimensional system with 2-component order parameter, the defects are the vortices which are the point defects (i.e, 0-dimensional), in 3-dimensional systems with 2-component order-parameter, the defects are strings or vortex lines (i.e, 1-dimensional), in 3-dimensional system with 3-component order parameter, the defects are monopoles (i.e, 1-dimensional). These different types of defects are shown in Figure 1.5.

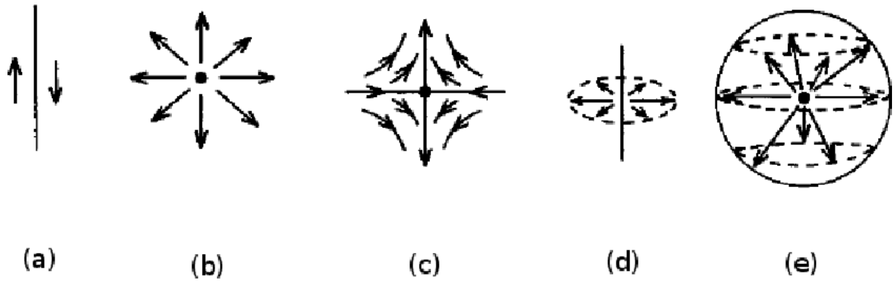

Figure 1.5: Schematic diagram of different types of topological defects. (a) One dimensional domain wall formed in two space dimensions (b) A zero dimensional vortex defect, in 2-space dimensions (c) An anti-vortex. (d) A vortex line in three dimensional space. (e) A monopole (of dimension zero) formed in d=3 space dimensions. Courtesy 'Kinetics of phase ordering'-A.J.Bray

We are particularly interested in the study of spiral patterns, which are more general defect structures of vortex variety, in reaction and spatial diffusions. So the discussion on the reaction-diffusion system and its modeling are discussed in the following sections. Before moving to that, below (see Fig.1.6) we provide a comparative picture of a vortex and spiral which will be useful for discussion of our results in subsequent chapters. Let us consider ordering of a 2-dimensional vector order parameter ($\psi = \rho e^{i\gamma}$) in $d = 2$. For a vortex defect, the lines for constant phases γ are radially outward from the core of the defect. On the other hand, for a spiral, these constant phase lines show bending, thus giving rise to phase gradient in the radial direction. This bending of the arms in a spiral destroys scaling property in various morphology characterizing functions, e.g., the two-point equal time correlation function, as we will see later.

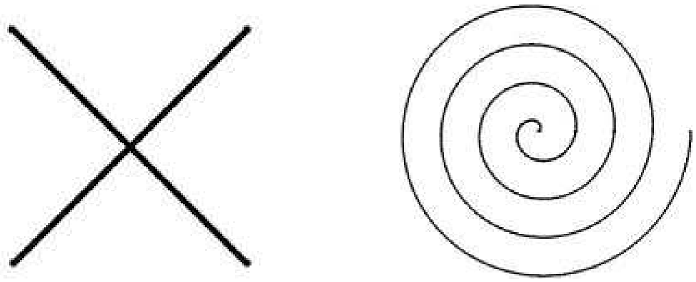

(a) Vortex (b) Spiral

Figure 1.6: (a) Four constant phase lines in a vortex defect. (b) One constant phase line in a spiral defect.

1.3 Some theoretical methods to study pattern formation

Pattern formation can be theoretically studied via Monte Carlo [26] or molecular dynamics [27] simulations of microscopic models, via approximate analytical or numerical solutions of coarse-grained dynamical equations [25], as well as via cellular automata [28]. For the sake of brevity, below we briefly discuss only the last two methods.

Coarse-grained dynamical equations: Typically the coarse-grained dynamical equations are obtained by writing down appropriate free energy functional and using it in Langevin equation. Below we provide one example, viz., the Swift-Hohenberg equation [1]. This will set the stage for the general discussion of reaction-diffusion systems. Note that the complex Ginzburg-Landau equation [1], on which the thesis is based, also represents reaction-diffusion systems. The Swift-Hohenberg equation is one of the well known equations to study pattern formation and is given by

$$\frac{\partial \psi(\vec{r},t)}{\partial t} = \mu\psi(\vec{r},t) - (\nabla^2+1)^2\psi(\vec{r},t) - \psi(\vec{r},t)^3 \tag{1.1}$$

where $\psi(\vec{r},t)$ is the space and time dependent order parameter of the system. Depending on value of the control parameter μ this equation exhibits hexagonal patterns or striped patterns. The striped patterns observed in Rayleigh-Bennard convection [1] can be studied by solving this equation. Time-evolution snap-shots obtained from numerical solutions of Swift-Hohenberg equation on a 2-d square lattice by fixing $\mu = 0.25$ is shown in Fig.1.7. This shows striped pattern.

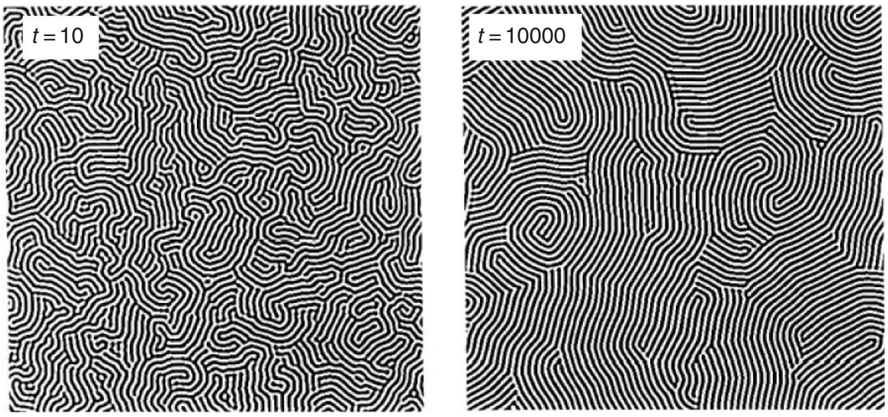

Figure 1.7: Time-evolution snap-shots obtained from simulation of Swift-Hohenberg equation on a 2-d square lattice of linear dimension $L = 256$ with $\mu = 0.25$. Courtesy: 'Pattern Formation and Dynamics in Nonequilibrium Systems'-Michael Cross and Henry Greenside.

Cellular automata: Cellular automata is an approach to study pattern formation on computers. In this method, one considers a regular grid of cells. There the cells can take only a discrete set of values. Starting from an initial state, some fixed rules depending on the state of the chosen cell and its neighbors are imposed on the cells. This determines the state of the system in next time step. This is a rather popular method to study pattern formation.

1.4 Reaction-diffusion system

This thesis deals with pattern formation in complex Ginzburg-Landau equation which belongs to the reaction-diffusion [1] variety. So, here we introduce the reaction-diffusion systems in more general context.

Reaction-diffusion systems are governed by some chemical reaction which causes transformation of one substance to another and further, the spatial diffusion of the reactants and the products due to space gradient. By the action of these two mechanisms patterns are formed. Despite the fact that it has been defined in the context of chemical systems, by no means reaction-diffusion systems are restricted to that.

Reaction-diffusion systems are mathematically represented as [1, 12]

$$\frac{\partial \psi(\vec{r},t)}{\partial t} = f(\lambda,\psi) + \nabla\cdot\left[D(\lambda,\psi)\nabla\psi\right] \tag{1.2}$$

where $\psi(\vec{r},t)$ is an order-parameter that may represent concentrations of one or multiple (providing the dimensionality of the order-parameter) chemical or biological species in the system, and λ represents some parameter such as a catalyst concentration. Here $f(\lambda,\psi)$ represents the reaction term, and the term involving the gradient operators represents diffusion with $D(\lambda,\psi)$ being the diffusivity of the system which may have dependence upon λ and ψ. As stated, ψ can have many different components thus representing the concentrations of multiple chemical or biological species. One can thus also introduce component dependent diffusivities to address more complex situations. For constant diffusivity, Eq.(1.2) becomes

$$\frac{\partial \psi(\vec{r},t)}{\partial t} = f(\lambda, \psi) + D\nabla^2\psi. \tag{1.3}$$

For diffusionless system $D = 0$. So in that case one simply works with reaction part

$$\frac{\partial \psi(\vec{r},t)}{\partial t} = f(\lambda, \psi). \tag{1.4}$$

1.5 Complex Ginzburg-Landau Equation

One of the extremely useful mathematical models which is extensively used to study dynamics of pattern formation in a variety of reaction-diffusion systems is the well known complex Ginzburg-Landau(CGL) equation [1,12]. The CGL equation is also extensively studied in nonlinear dynamics and has the general form

$$\frac{\partial \psi(\vec{r},t)}{\partial t} = \psi(\vec{r},t) + (1+i\alpha)\nabla^2\psi(\vec{r},t) - (1+i\beta)|\psi(\vec{r},t)|^2\psi_{(}\vec{r},t). \tag{1.5}$$

Here $\psi(\vec{r},t)$ is a 2-component vector or complex order parameter that depends upon space and time. This may represent concentrations of chemical substances in the system. Patterns are certainly observed due to the variation of order-parameter in space. Here α and β are some real parameters variations of which give rise to diversity in patterns. As already stated, the components of ψ can represent the concentrations of different chemical species. Then α, β are related to the catalyst concentrations and their diffusivities.

For $\alpha = 0, \beta = 0$, this equation reduces to the well studied real Ginzburg-Landau (RGL) equation [25, 29]

$$\frac{\partial\psi(\vec{r},t)}{\partial t} = \psi(\vec{r},t) + \nabla^2\psi(\vec{r},t) - |\psi(\vec{r},t)|^2\psi_(\vec{r},t). \tag{1.6}$$

This is often referred to as the dynamical XY model [25, 29] and is extensively used in the study of ordering in ferromagnet, superconductor, etc. RGL equation can directly be obtained from the Ginzburg-Landau free energy functional [25, 29]

$$F[\psi(\vec{r},t)] = \int d^3r \left[a\psi^2(\vec{r},t) + b\psi^4(\vec{r},t) + c(\bigtriangledown(\psi(\vec{r},t)))^2\right], \tag{1.7}$$

where the coefficients $a,\ b,\ c$ may have dependence upon temperature and other physical parameters. The functional derivative of this free energy $\frac{\delta F}{\delta\psi}$ provides a force in generalized sense. The rate at which an out of equilibrium system relaxes to equilibrium is assumed to be proportional to this generalized force. This is a valid approximation in slow dynamics situation and leads to the Langevin equation [25]

$$\frac{\partial \psi}{\partial t} = -\Gamma \frac{\delta F}{\delta \psi} \tag{1.8}$$

where the parameter Γ is related to the relaxation rate. Substitution of the expression of free energy from Eq.(1.7), into Eq.(1.8), leads to the RGL Eq.(1.6), for appropriate values of a, b and c.

For $\alpha, \beta \to \infty$, the CGL Eq.(1.5) reduces to the nonlinear Schrödinger equation [30] which has solitonic solutions. Note that RGL is a relaxational equation and the latter is Hamiltonian. The CGL is a bridging equation between the above two and does not have a free energy functional in general.

Despite the complex nature, the CGL equation has some approximate analytical solution [12, 31] in the single spiral situation (note that this equation exhibits spiral pattern for large ranges of the parameter values α and β). This we will discuss subsequently when we present results.

1.6 Overview of the Thesis

In this thesis, we aim to study pattern formation in the CGL equation and compare the results with the RGL equation. Of special interest is the case $\alpha = \beta$ and the effect of disorder [32, 33] in α and β in the dynamics. It is well known that for $\alpha \neq \beta$, the CGL equation exhibits statistically frozen spiral dynamics [8–10]. We want to investigate what effect the above mentioned disorder can have on the dynamics. This latter study is motivated by disorder mediated studies in scalar order-parameter systems [34–36], e.g., in Ising model.

To achieve the objective, we have solved the CGL equation numerically applying simple Euler discretization method [37]. In this method, a partial differential equation

$$\frac{\partial P}{\partial t} = X(P) \tag{1.9}$$

is solved as

$$P_{t+\Delta t} = P_t + \Delta t X(P_t), \tag{1.10}$$

where the subscripts t and $t + \Delta t$ represent the value of P at times t and $t + \Delta t$. Here, we have calculated the Laplacian (that appears in the CGL equation) as

$$\nabla^2 P = \left(\sum_i P_i - nP_o \right) / (\Delta x)^2, \tag{1.11}$$

where the summation is over the nearest neighbors, n is the number of nearest neighbors and o is the central site. In Eqs.(1.10) and (1.11),

Δt and Δx are discretization in time and space. One needs to choose reasonably small values for these quantities to obtain stable solutions of the equations.

Bibliography

[1] M. C. Cross and P. C. Hohenberg, Rev. Mod. Phys., **65**, 851 (1993).

[2] E. P. Zemskov, V. K. Vanag and I. R. Epstein, Phys. Rev. E, **84**, 036216 (2011).

[3] V. K. Vanag and I. R. Epstein, Science, **294**, 835 (2001).

[4] E. M. Nicola, L. Brusch and Bär M., Phys. Chem. B, **108**, 14733 (2004).

[5] M. Hemmele, S. Schuler and W. Zimmermann, Physica D, **218**, 139 (2006).

[6] M. Hendrey, E. Ott and T. M. Antonsen jr, Phys. Rev. Lett., **82**, 859 (1999).

[7] M. Hendrey, E. Ott and T. M. Antonsen jr, Phys. Rev. E, **61**, 4943 (2000).

[8] S. K. Das, Puri S. and Cross M. C., Phys. Rev. E, **64**, 046206 (2001).

[9] Puri S., S. K. Das and M. C. Cross, Phys. Rev. E, **64**, 056140 (2001).

[10] S. K. Das, S. Puri, Phys. Rev. E, **65**, 046123 (2002).

[11] A. M. Turing, Royal Society of London, **237**, 641 (1952).

[12] I. S. Aranson and L. Kramer, Rev. Mod. Phys., **74**, 99 (2002).

[13] R. A. Bagnold, *The Physics of Blown Sand and Desert Dunes* Metheun (1941).

[14] R.P. Sharp, J. Geol., **71**, 617 (1963).

[15] I.G. Wilson, Sedimentology, **19**, 173 (1972).

[16] K. Pye, H. Tsoar, ,*Tsoar, Aeolian Sand and Sand Dunes*, Unwin Hyman, London, (1990).

[17] R. Cooke, A. Warren, A. Goudie, *Desert Geomorphology*, UCL Press, London, (1993).

[18] N. Lancaster, *Geomorphology of Desert*, Routledge, New York, (1995).

[19] J.F. Kennedy, Ann. Rev. Fluid Mech., **1**, 147 (1969).

[20] F. Brugmans, Earth Surf. Proc. Landforms, **8**, 527 (1983).

[21] M. Matchinski, La Nature, **3241**, 169 (1955).

[22] R. S. Anderson, Sedimentology, **34**, 943 (1987).

[23] R. S. Anderson, Earth Sci., **29**, 77 (1990).

[24] *Chemical Waves and Patterns*, edited by R. Kapral and K. Showalter (Kluwer Academic, Dordrecht, 1993).

[25] A.J. Bray, Adv. Phys., **51**, 481 (2002).

[26] D. P. Landau and K. Binder, *A guide to Monte Carlo Simulations in Statistical Physics* (Cambridge University Press, Cambridge, 2009).

[27] D. Frenkel and B. Smith, *Understanding Molecular Simulations: From algorithim to applications* (Academic Press, San Diego, 2002).

[28] S. Wolfram, Rev. Mod. Phys. **55**, 601 (1983).

[29] N. Goldenfeld, *Lectures on Phase Transitions and the Renormalization Group* (Levant Books) 2005.

[30] A. C. Newell, *Solitons in Mathematics and Physics*, CBMS Lect. Ser., Vol **48** (SIAM Press, Philadelphia) 1983.

[31] P. S. Hagan, SIAM J. Appl. Math., **42**, 762 (1982).

[32] S.K. Das, Europhys. Lett., **97**, 46006 (2012).

[33] S.K. Das, Phys. Rev. E, **87**, 012135 (2013).

[34] D. A. Huse and C. L. Henley, Phys. Rev. Lett. **54**, 2708 (1985).

[35] S. Puri and N. Parekh, J. Phy. A: Math. Gen.**26**, 2777 (1993).

[36] F. Corberi, E. Lippiello, A. Mukherjee, S. Puri and M. Zannetti, J. Stat. Mech. P03016 (2011).

[37] R. De Carlo, *Linear Systems: A state variable approach with numerical implementation* (Prentice Hall, New Jersey, 1989).

Chapter 2

A Comparative Study of Pattern and Dynamics in Complex and Real Ginzburg-Landau Equations

2.1 Introduction

The complex Ginzburg-Landau (CGL) equation [1–3] has the general form

$$\frac{\partial \psi(\vec{r},t)}{\partial t} = \psi(\vec{r},t) + (1+i\alpha)\nabla^2\psi(\vec{r},t) - (1+i\beta)|\psi(\vec{r},t)|^2\psi(\vec{r},t), \quad (2.1)$$

where ψ is a space ($\vec{r}$) and time (t) dependent complex order parameter [$\psi(\vec{r},t) = \rho(\vec{r},t)e^{i\gamma(\vec{r},t)}$, ρ being the amplitude and γ the phase] and α, β are real parameters. With the variation of the parameters α and β, the CGL equation exhibits a variety of interesting patterns and dynamics. The equation has two interesting limiting forms. For $\alpha = \beta = 0$, one has

$$\frac{\partial\psi(\vec{r},t)}{\partial t} = \psi(\vec{r},t) + \nabla^2\psi(\vec{r},t) - |\psi(\vec{r},t)|^2\psi(\vec{r},t), \tag{2.2}$$

which we will refer to as the real Ginzburg-Landau (RGL) equations. Often in the literature of phase ordering dynamics, the RGL is referred to as the dynamical XY model [4, 5]. This latter nomenclature is due to the fact that ψ is a two-component vector order parameter and the corresponding Hamiltonian is same as the XY model.

The RGL exhibits relaxational dynamics where the pattern is characterized by vortices and antivortices [4]. Starting from the Ginzburg-Landau (GL) hamiltonian or free energy [4]

$$F[\psi(\vec{r},t)] = \int d^3r \left[-|\psi|^2 + (\bigtriangledown\psi)^2 + |\psi|^4\right], \tag{2.3}$$

the RGL can be obtained from the Langevin equation [6]

$$\frac{\partial \psi}{\partial t} \propto -\frac{\delta F}{\delta \psi}, \tag{2.4}$$

in the slow dynamics approximation. In space dimension $d = 2$, these above mentioned vortices and antivortices are point defects where the constant phase lines move radially outwards from the defect cores [4]. These defects interact with each other via Coulomb potential [7]. Because of this, the defects and anti-defects annihilate each other. This orders the system and lowers the energy. In $d = 3$, such point defects from different planes meet and the cores form lines which we will refer to as vortex lines [4].

In another limit $\alpha = \beta = \infty$, the CGL equation becomes

$$i\frac{\partial \psi}{\partial t} = \nabla^2 \psi - |\psi|^2 \psi, \tag{2.5}$$

which is the well known nonlinear Schrödinger (NLS) equation [8]. This equation provides solitonic solution and is nondissipative.

Both RGL and NLS are analytically better tractable than the general one, i.e., the CGL equation. Nevertheless, there exists some approximate analytical solution and analysis for the CGL equation as well [3, 9], in the single defect limit. The CGL equation can be thought of as a system of coupled oscillations. In its general form, the equation provides spiral pattern in the phase field of the order parameter [1]. This equation is used for general understanding of spiral pattern observed in a variety of interesting physical systems [1]. An interesting and important example is the Belouzov-Zhabotansky (BZ) chemical reaction [10] where constant concentration of certain chemical species form spiral pattern in space which oscillates in time. In the context of the BZ reaction, the parameters β and α can be related to the catalyst concentration and diffusivity.

The dynamics of RGL equation is rather well studied. Note that the vortex pattern that this equation exhibits is a special case of spiral, as expected. Essentially, for a vortex the constant phase lines move radially outward from the core of the defect whereas in case of spirals they wind or exhibit bending around the centre or core. The characteristic length scale, $\ell(t)$, which can be thought of as the average length under a defect, diverges for RGL with time as [4]

$$\ell(t) \sim t^{1/z}, \tag{2.6}$$

with $z = 2$. In $d = 2$, of course, a logarithmic correction is predicted [4]. However, in computer simulations it is extremely difficult to probe such weak correction.

The pattern formation in various dynamical systems is characterized by the two-point equal time correlation function [4]

$$C(r = |\vec{r_1} - \vec{r_2}|, t) = Re < \psi(\vec{r_1}, t)\psi^*(\vec{r_2}, t) >, \tag{2.7}$$

where $\psi^*(\vec{r_2}, t)$ is the complex conjugate of the order parameter field at $\vec{r_2}$ at time t. In case of RGL, the analytical form of such correlation function is due to Bray, Puri and Toyoki (BPT) [4, 11, 12] which has the form

$$C(r,t) = \left[\frac{e^{-r^2/2\ell^2}}{\pi}\right]\left[B\left(\frac{3}{2}, \frac{1}{2}\right)\right]^2 F\left(\frac{1}{2}, \frac{1}{2}; 2; e^{-r^2/\ell^2}\right), \tag{2.8}$$

where $B(a, b)$ is the Beta function and $F(e, f; g; h)$ is the hypergeometric function [13]. Eq.(2.8) describes the multi-defect morphology in RGL rather remarkably. On the other hand, it has been possible to obtain the semi-analytical form of $C(r, t)$ for the CGL equation only in single spiral limit [14]. The latter however appears to be a reasonable description of multi-spiral pattern.

The single spiral oscillatory solution for the CGL equation is written as [3, 9]

$$\psi(\vec{r}, t) = \rho(r) \exp[-i\omega t + i\theta - i\phi(r))]. \tag{2.9}$$

It is clear that for nonzero value of frequency ω, Eq.(2.9) provides traveling wave. The limiting forms of ρ and ϕ in Eq.(2.9) are given as

$$\rho(r) \to ar,\ r \to 0;\ \ \to \sqrt{1-q^2},\ r \to \infty \tag{2.10}$$

$$\phi'(r) \to r,\ r \to 0;\ \ \to q,\ r \to \infty \tag{2.11}$$

where a is a constant and the parameter q can be obtained from the knowledge of ω, α and β as

$$q = \sqrt{\frac{\omega - \beta}{\alpha - \beta}}. \tag{2.12}$$

In Eq.(2.12), ω, that depends upon α and β, can be obtained from numerical experiments as we will discuss later [14].

For the RGL equation ($\alpha = \beta = 0$), $\omega = 0$ and one obtains stationary solution [1, 3]. There, of course, $\phi'(r)$ is also zero. Note that $q = \phi'(r)$ represents the gradient of the total phase in the radial direction which, in case of a vortex, is by definition absent. However, for a vortex structure ω need not be zero in general - the only requirement is that q must be zero. From more general analysis [3], it appears that, for $\alpha = \beta = \lambda$ (from here on usage of λ will indicate that $\alpha = \beta$), the defect structure is vortex, even though for $\lambda \neq 0$, $\omega \neq 0$. In that case, one can naturally ask, is the dynamics for $\lambda \neq 0$ is similar to $\lambda = 0$, i.e., the RGL equation, as well as the corresponding patterns in multi-defect situation? Here we note that, in general, for $\alpha \neq \beta$, it is understood that, in the multi-defect context, CGL exhibits frozen dynamics [2,14–16]. Essentially, as opposed to the RGL where the interaction between a vortex and anti-vortex is all along Coulombic, there is a repulsive barrier in case of spiral and anti-spiral interaction beyond a certain distance [1]. This does not allow such pairs to approach each other below that characteristic length scale of the system. In this work, via numerical solution of the CGL equation on a square ($d = 2$) and simple cubic ($d = 3$) lattice systems, we verify, if that is also true for $\lambda \neq 0$ and if not, how similar the dynamics is, for general values of λ, compared to the RGL equation. While we have carried out studies for multiple nonzero values of $-2 \leq \lambda \leq 2$, for the sake of brevity, we will present detailed results only for $\lambda = \pm 1$. In addition, we also verify the single spiral solution for rather general values of α and β.

The rest of the chapter is arranged as follows. We discuss the details of numerical methods in Section 2.2. Results are presented in Section 2.3. Finally the chapter is concluded with a brief summary of results in Section 2.4.

2.2 Methodology

We have solved the CGL equation either on a square lattice or a simple cubic lattice depending upon whether we are working in $d = 2$ or $d = 3$. We have implemented the standard Euler discretization technique to solve the equations. Periodic boundary conditions were applied in all directions.

The characteristic length scale or the average defect size, $\ell(t)$, was calculated from two different methods. Note that in ordering dynamics the correlation function $C(r, t)$ exhibits the scaling behavior [4]

$$C(r, t) \equiv \tilde{C}(r/\ell(t)), \tag{2.13}$$

where $\tilde{C}(x)$ is a master function independent of time. This behavior of $C(r, t)$ reflects the self-similar nature of pattern formation, essentially meaning that the structure at different times are equivalent, differing only by a change in length scale. We have used this scaling property, as a method of calculation of $\ell(t)$. Essentially, in this method we obtained $\ell(t)$ from the distance at which $C(r, t)$ decays to 1/2 its maximum value. In case of vortex pattern it is well known that the scaling property in Eq.(2.13) holds good [4]. However for spirals there is no such structural scaling [14] and so we need to introduce another method for the calculation of $\ell(t)$. In this second method we have calculated the number of defects $N(t)$ at a time t by identifying a defect with the condition [4]

$$\oint d\gamma = 2\pi m, \tag{2.14}$$

where m is a +ve or -ve integer. Basically, for a point in space, if the sum of phase changes along the smallest loop around the point under consideration is an integral multiple of 2π, then there is a defect inside the loop. This way, sweeping through the whole lattice, $N(t)$ can be calculated. Once we have the knowledge about $N(t), \ell(t)$, e.g., in $d = 2$ can be obtained as

$$\ell(t) = \frac{L}{\sqrt{N(t)}}, \tag{2.15}$$

where L is the linear dimension of the system under study.

Further to characterize the growth law, in addition to using standard methods, we have calculated the instantaneous exponent [17]

$$\frac{1}{z_i} = \frac{d \ln \ell(t)}{d \ln t}. \tag{2.16}$$

This, of course, is appropriate for the assumption that we are dealing with power-law growth [see Eq.(2.6)]. The calculation of the instantaneous exponent is often useful considering the fact that there may be deviation of the exponent at early time for various reasons. E.g., for scalar order parameter with conserved order-parameter dynamics the curvature of small domains at early time can give rise to correction [17] and in that case it becomes necessary to take a limit $\ell \to \infty$ to obtain information about the value of z_i in this asymptotic limit. Here, of course, we are dealing with a nonconserved order parameter. Such correction may be present in the nonconserved dynamics also. However, due to much faster growth in this case (compared to the conserved dynamics), not much difficulty is usually encountered in realizing the true asymptotic value.

In the Euler discretization method, unless otherwise mentioned, we have used $\Delta t = 0.01$ and $\Delta x = 1$ throughout the thesis. All the observables or physical quantities were calculated from averaging over 10 independent initial configurations for $L = 256$ in $d = 2$ and $L = 128$ in $d = 3$.

2.3 Results

This section is divided into two subsections. In the first one we present results in $d = 2$ and the results for $d = 3$ are presented in the second subsection.

2.3.1 d=2

In Fig.2.1 we present the evolution snapshot for the 2-d CGL equation with $L = 256$ and periodic boundary conditions in both $x-$ and $y-$ directions, starting from a specially prepared vortex initial configurations, core of which is located at the centre of the lattice system. The different colors in the snapshots correspond to phase values $\gamma = 0$ and π. With passing time, spiral nature of the defect becomes prominent and area under the spiral also increases. Here note that, due to discrete nature of the lattice and small size of the system, in order to make the look of the spiral arms continuous, we have used an width of 0.4 around the mean value of phase. The values of α and β, in this case, was fixed to 1.0 and 0 respectively. From the snapshots at different times, it is also clear that these spirals are traveling waves.

Even though we have started with a single defect at the centre of the system, it appears that there are other defects in the boundary region of the system. This is due to the application of periodic boundary conditions that allow images. These peripheral spirals collide with the central one and form the so called "shock defect" [2].

Next to test the single spiral solution [see Eqs. (2.9),(2.10),(2.11),(2.12)], in Fig.2.2 we present a plot of $\rho(x)$, corresponding to the last snapshot in Fig.2.1, as a function of x, by fixing $y = L/2$, i.e., for the horizontal line passing through the centre of the central defect. It appears that starting from small value at the centres of the defects ρ saturates or tries to settle

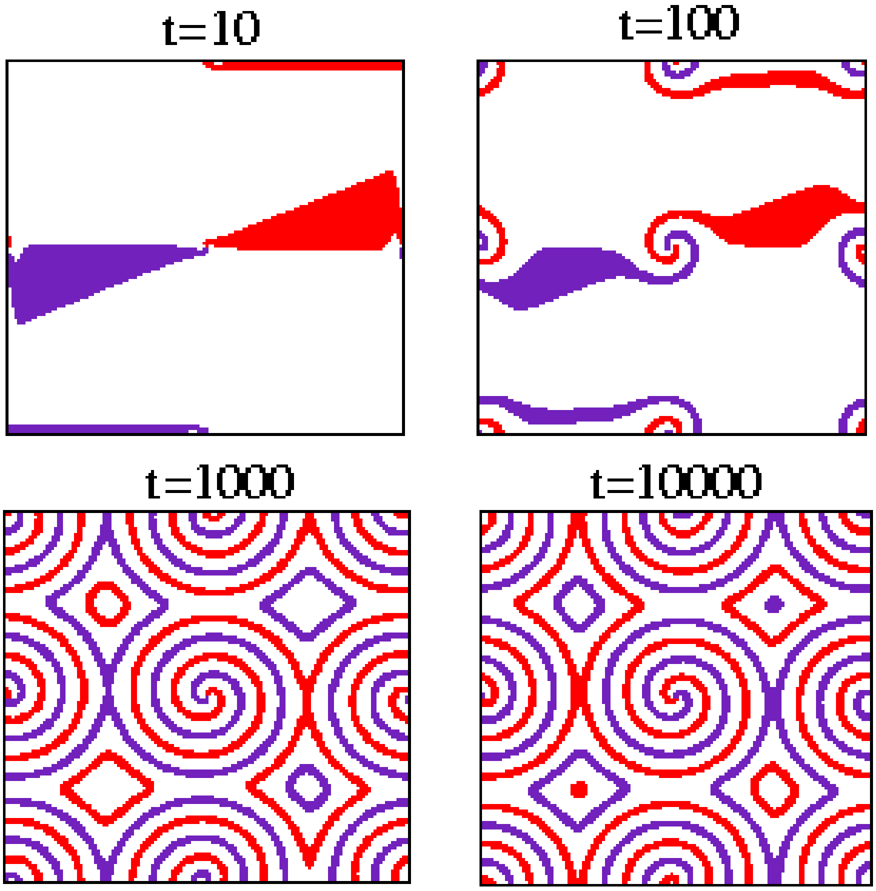

Figure 2.1: Snapshots during the evolution of spiral(s) obtained via numerical solutions of the complex Ginzburg-Landau equations on a 2-d square lattice, starting from an artificially created vortex initial configuration with the core located at the centre of the lattice system. Periodic boundary conditions were used in both x- and y-directions. In numerical solutions we have set the sizes Δx and Δt to 1 and 0.01. The different colors correspond to the phase values $\gamma = 0$ and π with some width around these mean values so that the lines look continuous. We have fixed the values of α and β to 1 and 0, respectively. The linear dimension of the system is $L = 256$. Pictures from four different times are presented.

to a constant asymptotic value far away from the defect core. But in the regions where two defects collide, it shows a (smooth) jump [2]. We will examine the asymptotic value later. Before that, in Fig.2.3, we take

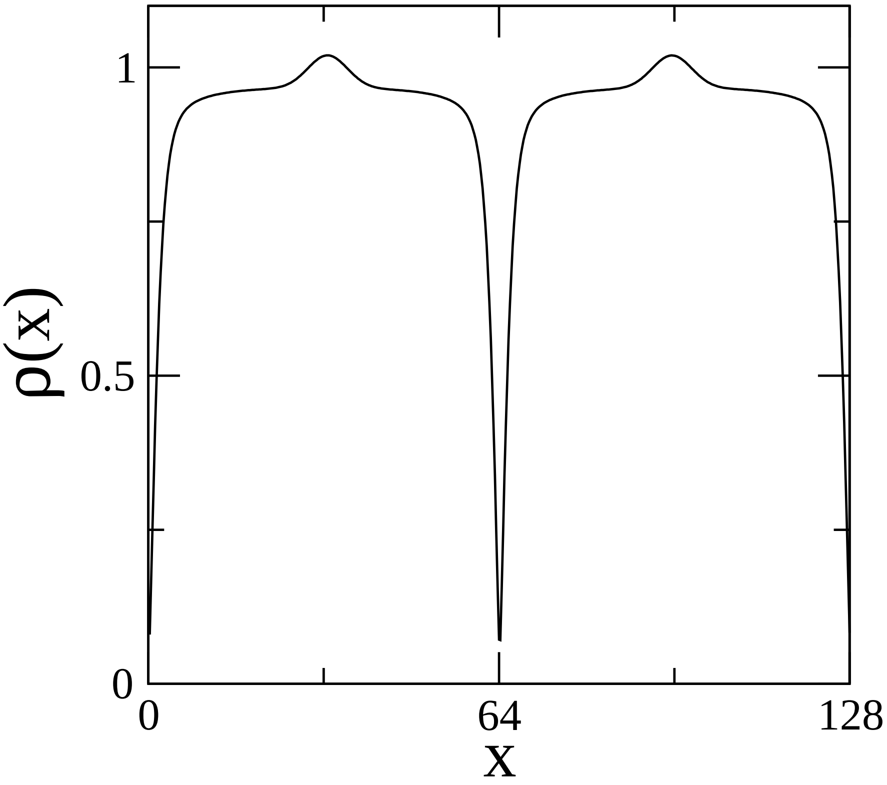

Figure 2.2: Plot of the order-parameter amplitude ρ as a function of the x coordinate of Fig.2.1, by fixing $y = L/2$. This plot corresponds to the latest time picture of Fig.2.1.

a closer look at ρ in the vicinity of the core. In this picture we have shifted the $x-$coordinate so that the core appears at $x = 0$. The dashed line in the figure is a straight line. It is clearly seen that the behavior of ρ, for $x \to 0$, is nicely consistent with this dashed line. This confirms one

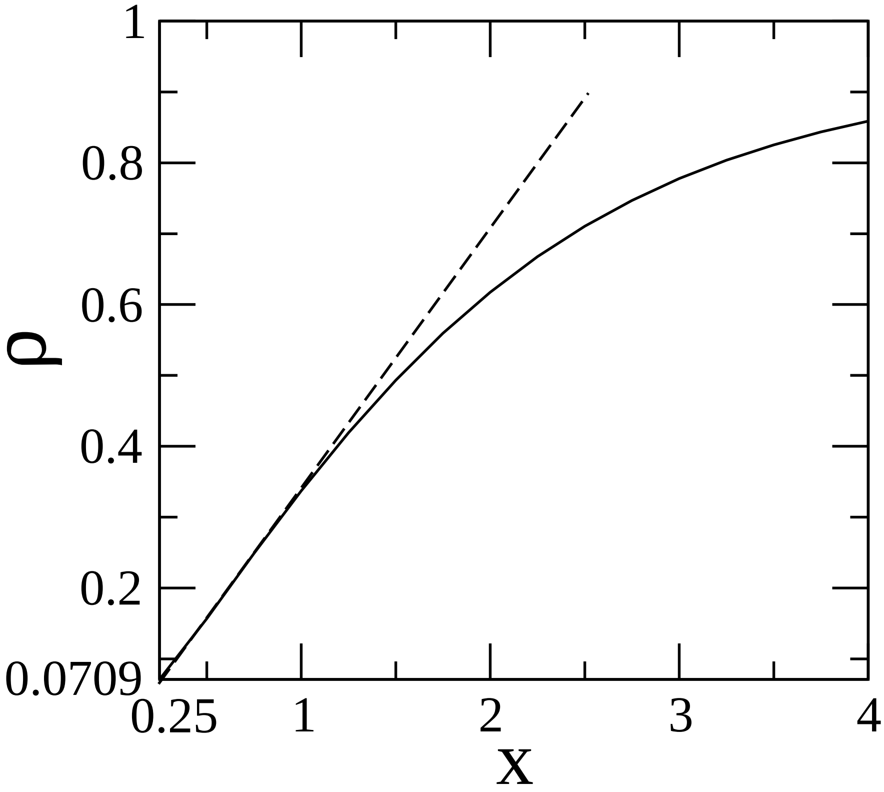

Figure 2.3: Close up of Fig.2.2, focusing in the core the region of the central spiral. The dashed line represents expected linear behavior of ρ in this region.

of the predictions of the single spiral approximate analytical solution, of course.

In Fig.2.4, we show the variation of overall phase γ as a function of t for a point inside the central spiral of Fig.2.1 but reasonably away from the core. It is clearly seen that this is periodic and from the time period of this oscillation, we calculate the frequency ω. Further, using ω in Eq.(2.12), we calculate the value of q. Now we are in a position to check

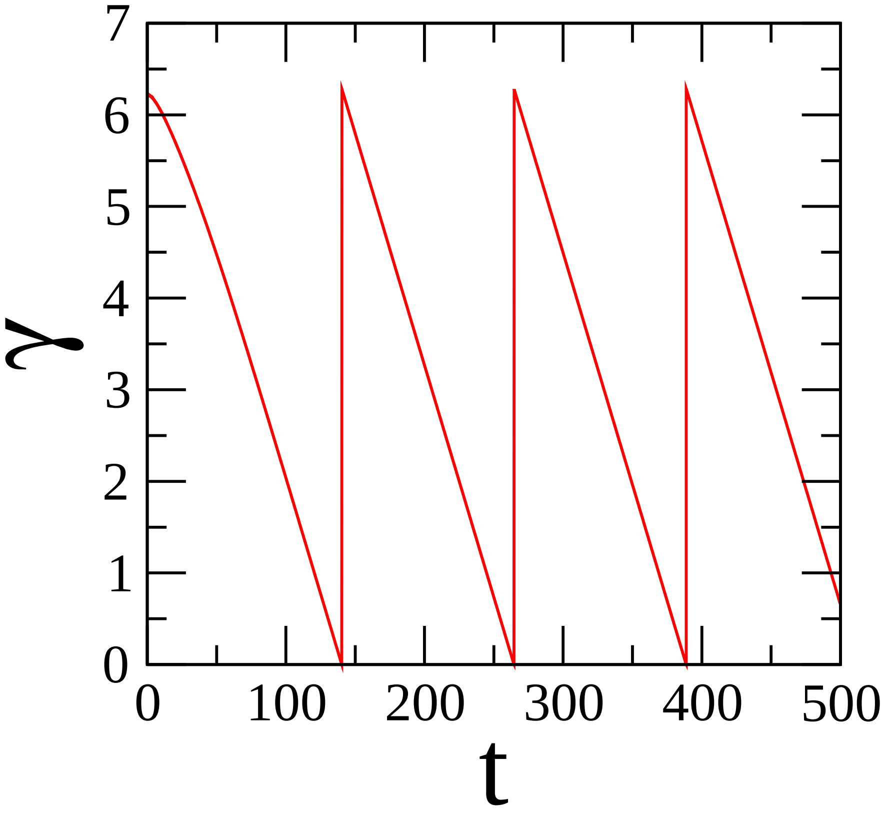

Figure 2.4: Plot of phase γ vs t, for a site far away from the core but within the central spiral of Fig.2.1.

the prediction of single spiral solution for ρ in the limit (r or) $x \to \infty$.

In Fig.2.5(a), we replot Fig.2.2 but in this case the value of the ordinate for $\rho = \sqrt{1-q^2}$ is marked by the dashed line. It is quite clear that far away from the core, ρ is approaching towards $\sqrt{1-q^2}$ thus verifying another prediction of the single spiral solution. In Fig.2.5(b) we show a similar figure for $\alpha = 0, \beta = 1$ where also such consistency is seen. This latter case, i.e., $\alpha = 0,\ \beta = 1$ was varified in another recent study [18].

In Fig.2.6, we replot the snapshots of Fig.2.1 but here we have shaded the region where $\rho > \sqrt{1-q^2}$. It appears that in the region where spiral nature of the defects is prominent $\rho < \sqrt{1-q^2}$. From the two latest time snapshots, it is evident that in the "shock region", where two defects meet, ρ assumes values greater than $\sqrt{1-q^2}$. Recently it has been pointed out that such behavior of ρ may be responsible for the appearance of repulsive barrier [18]. Finally, the single spiral solution appears to be good even for multi-spiral morphology (note that due to the periodic boundary condition, effectively we obtained a multi-defect structure despite starting from a single defect initial configuration), but this solution does not provide information in the shock region. It was recently observed that if the amplitude in the shock region (in special case for $\alpha = 0$ and varying only β) is artificially suppressed to $\sqrt{1-q^2}$, the spirals are able to interact again and in that case the pattern and growth of the system is very similar to the RGL [18].

Having discussed about the pattern and dynamics starting from single

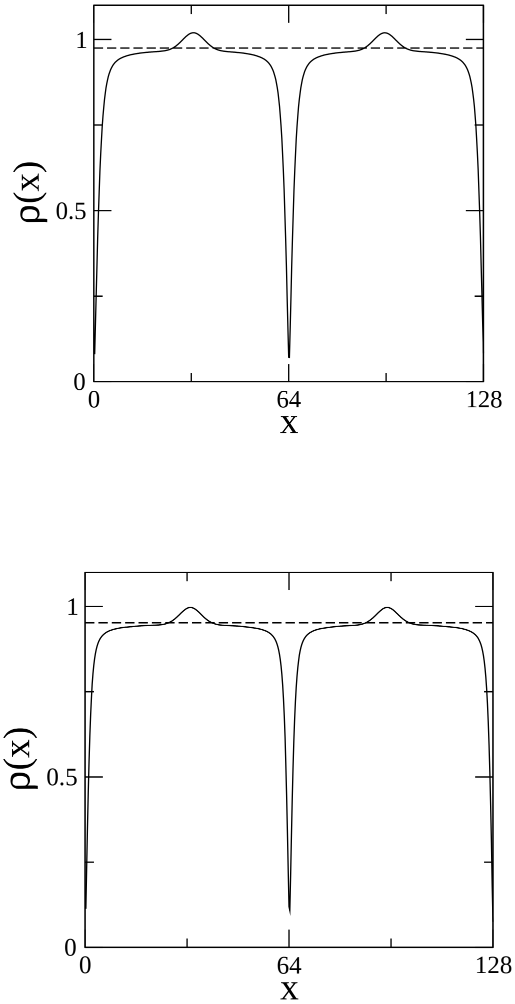

(b)

Figure 2.5: (a) Re-plot of Fig.2.2 to investigate the value of ρ far away from the spiral core. The horizontal dashed line here has value $\rho = \sqrt{1-q^2}$, $q = 0.2223$ for $\alpha = 1, \beta = 0$. (b) Same as (a) but for $\alpha = 0,\ \beta = 1$ ($q = 0.306$).

defect initial configuration, now we move on to multi-spiral case. Note that multi-defect morphology can be obtained by starting from initial configurations random in both amplitude and phase.

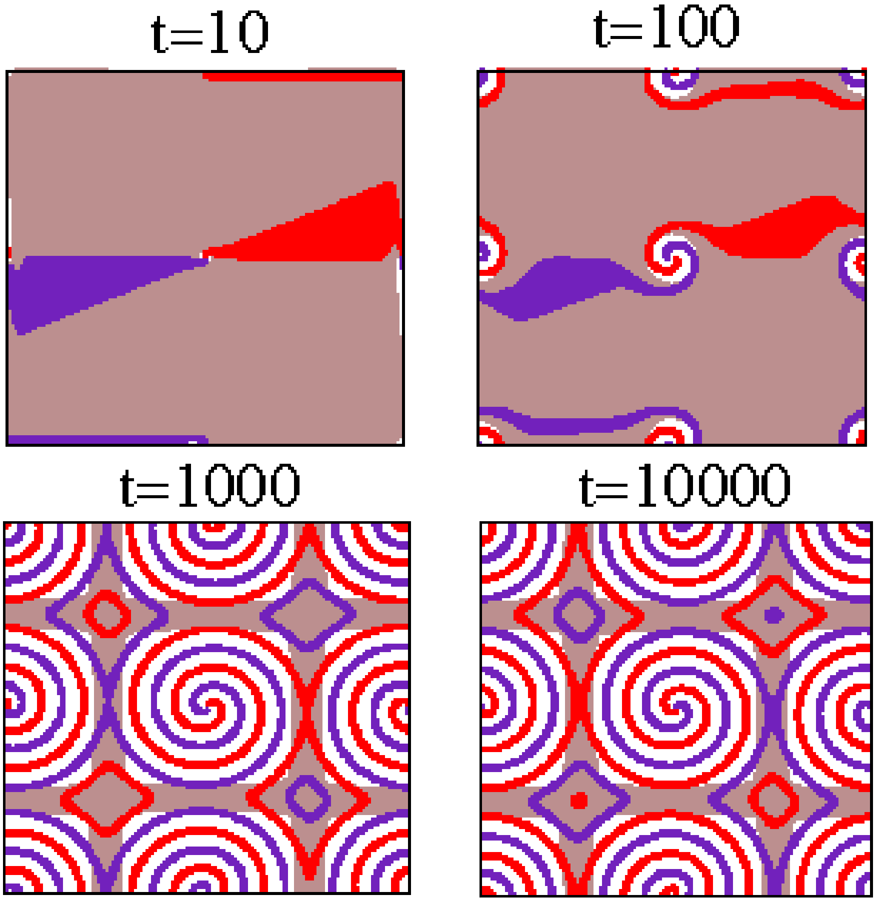

Figure 2.6: Same as Fig.2.1 but here the region where ρ is greater than $\sqrt{1-q^2}$ is shaded.

In Fig.2.7 we present the snapshots for the evolution starting from random initial configurations. Again we have set $\alpha = 1, \beta = 0$ and $L = 256$. The color coding here has similar meaning as earlier. The black dots in this picture represent the defect cores and were determined by the method described in the previous section. It is clearly seen that starting from very high defect density the system orders in time. However, the snapshots at $t = 1000$ and 10000 gives the impression of a frozen dynamics [2, 14–16] since not much change has happened over this long period of time.

To compare the pattern of Fig.2.7 with the RGL, in Fig.2.8 we present similar snapshots, again starting from random initial configuration, for $\lambda = 0$. It appears that there is no regular bending of the constant phase lines as in the spiral case. Here emerging from the defect cores (where two different colors meet), these lines are radially outward (with respect to the coordinate system having origin at the cores of the defects). The random bending, observed far away from cores, is due to the inter defect interaction.

Coming to the primary objective of this chapter, i.e., a general study of pattern dynamics in the CGL equation for $\alpha = \beta = \lambda$, in Fig.2.9 we show evolution snapshots for $\lambda = -1$. The nature of the pattern here and the RGL equation (see Fig.2.8) is very similar. In addition, here also it is seen that the vortices and anti-vortices are continuously annihilating each other and the system is evolving towards a perfectly ordered state

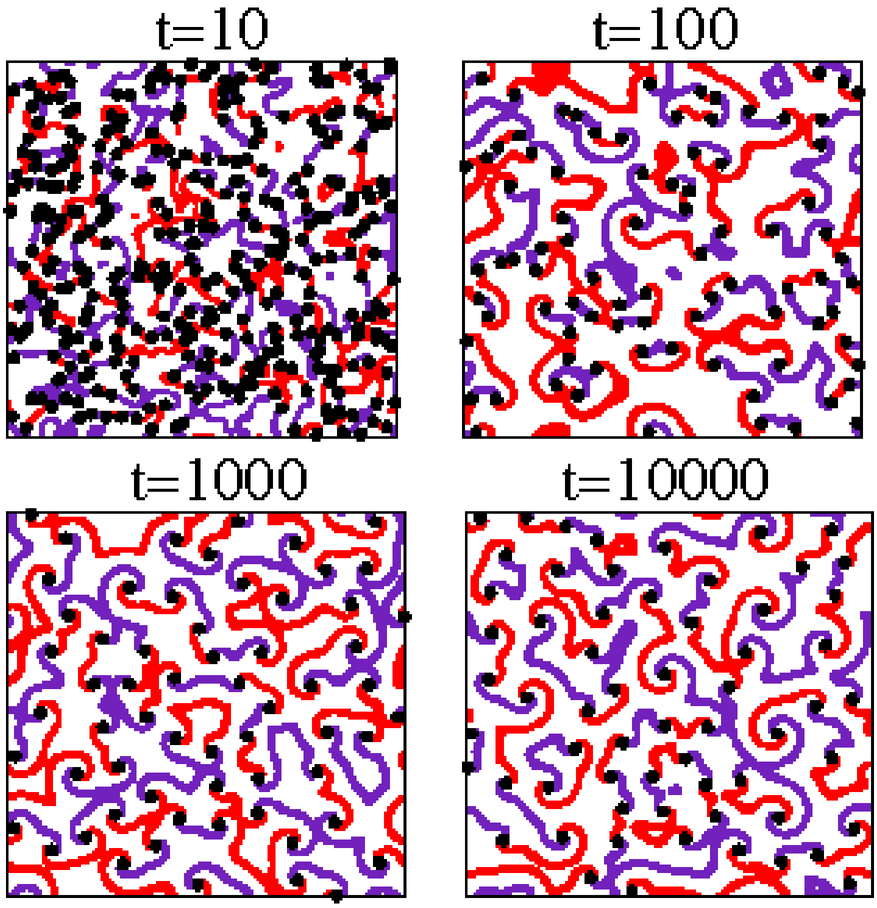

Figure 2.7: Snapshots from four different times during the evolution of the CGL equation with $\alpha = 1, \beta = 0; L = 256$, starting from random initial configuration, using periodic boundary conditions. The color coding is same as Fig.2.1. The values of Δx and Δt were set to 1 and 0.01, respectively. The black dots mark the location of the defect cores.

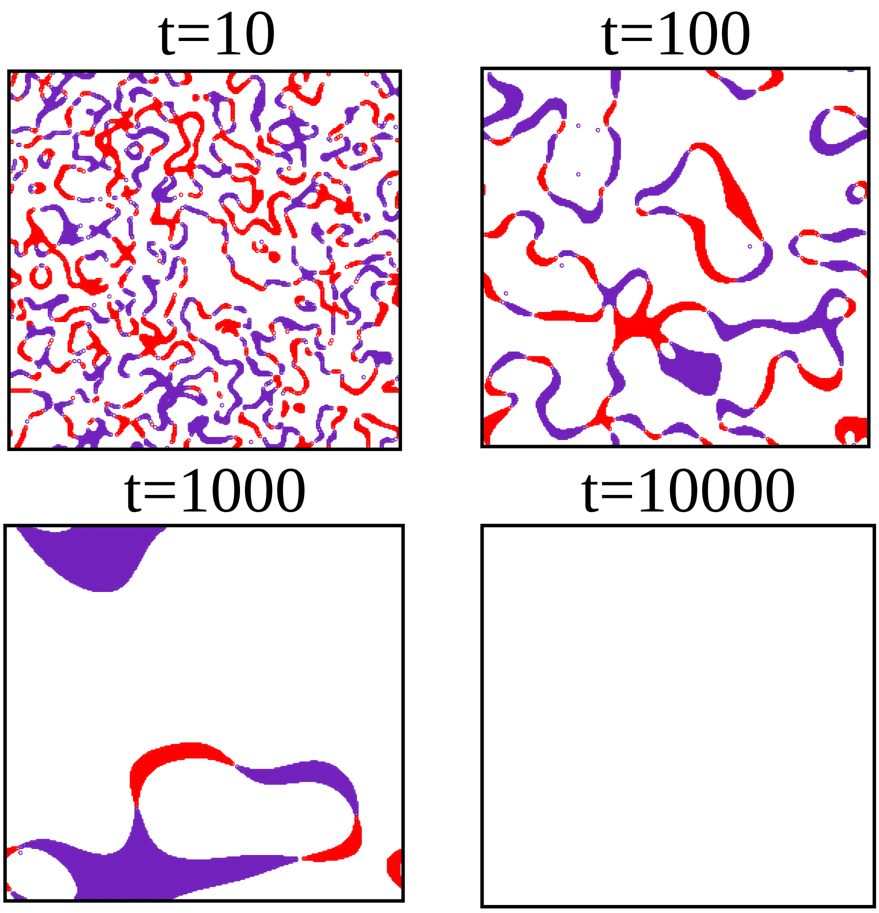

Figure 2.8: Same as Fig.2.7 but for $\alpha = \beta = 0$

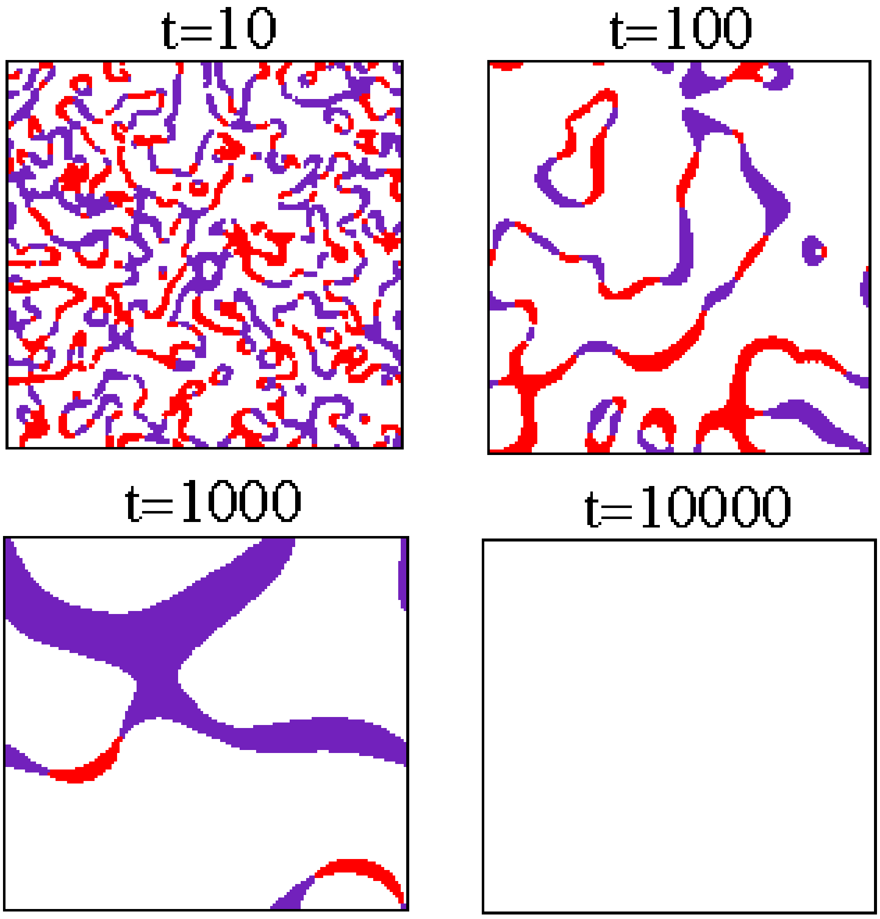

Figure 2.9: Same as Fig.2.7 but for $\alpha = \beta = -1$

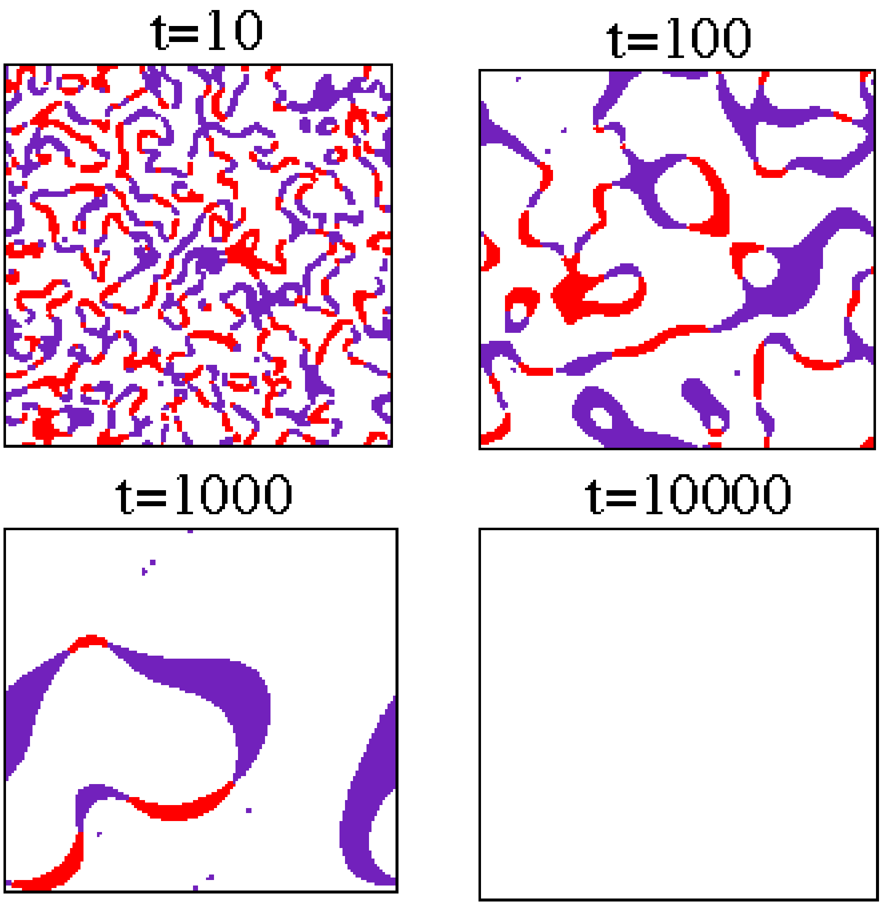

Figure 2.10: Same as Fig.2.7 but for $\alpha = \beta = 1$

without any defect. Note that an empty box (also in Figs.2.8 and 2.10) corresponds to a defect-free system. Analogous snapshots are shown in Fig.2.10, for $\lambda = 1$. Here also the basic pattern and dynamics are same as the RGL equation. Here again, we recall that the equations for $\lambda \neq 0$ is different from the RGL equation. The single spiral solution for general values of λ, of course, predicts that $q = 0$. It is interesting, nevertheless, to note that the structure in multi-defect context also remains similar despite the rotational motion for nonzero value of λ giving nonzero frequency ω.

To compare the morphology at a qualitative level, in Fig.2.11 we have shown the correlation functions from $\lambda = 0, 1$ and -1, from late time configurations. It is seen that results from all different values of λ are in nice agreement with each other. In this figure, we have also shown the BPT function which nicely passes through the numerical data points.

To quantify the dynamics, in Fig.2.12 we plot $\ell(t)$ as a function of time, on a double linear scale. Data for $\alpha = \beta = 0, -1, 1$ and $\alpha = 1, \beta = 0$ are included. All results in this figure correspond to the calculation from the decay of the correlation functions.

As already pointed out, for $\alpha \neq \beta$ (viz., $\alpha = 1, \beta = 0$), $\ell(t)$, after a certain time, does not grow, implying that the system is locked in a frozen state. On the other hand, for all values of $\alpha = \beta$, $\ell(t)$ continuously increases. It appears that for nonzero value of λ, the growth is faster than the RGL. This enhanced growth may be due to the higher value of ampli-

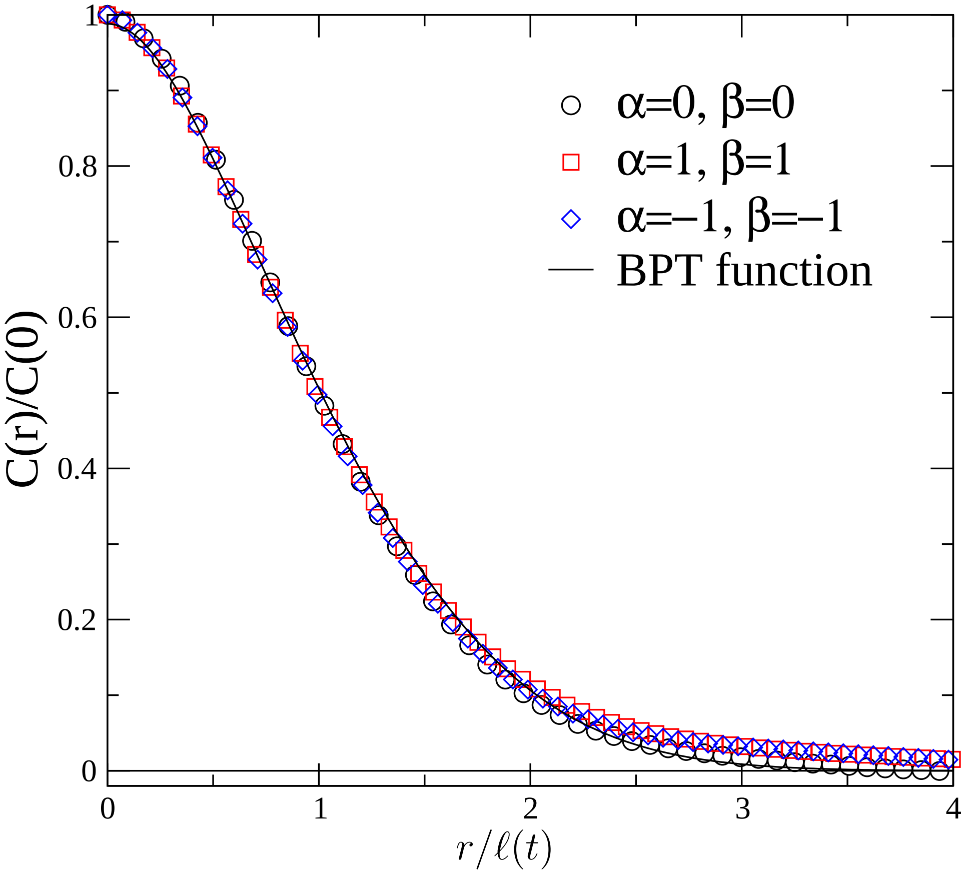

Figure 2.11: Plots of correlation functions, $C(r,t)$, vs the scaled distance $r/\ell(t)$, from t=250 for $\alpha = \beta = 0, -1, 1$. The length scale $\ell(t)$ was obtained from the distance where $C(r,t)$ decays to 0.5 its maximum value. The continuous line represents the Bray-Puri-Toyoki form of $C(r,t)$.

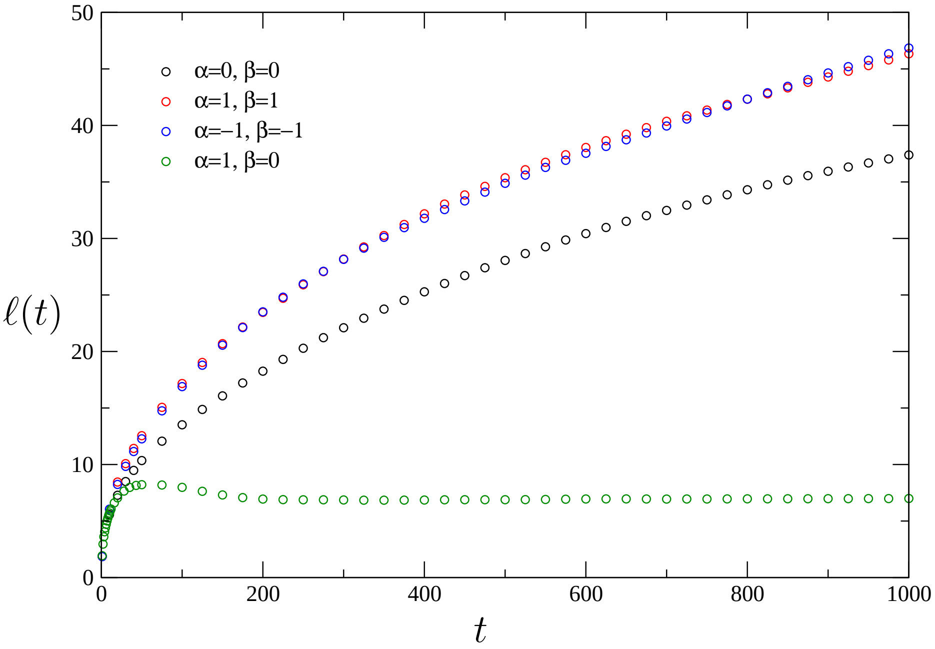

Figure 2.12: Plots of $\ell(t)$ vs t for four different cases, viz., $\alpha = \beta = -1, 0, 1$ and $\alpha = 1, \beta = 0$. A linear scale is used. In all the cases the data were obtained from the decay of the two-point equal time correlation functions.

tude or exponent which we will check later. Another observation is that the dynamics for $\lambda = \pm 1$ is very similar [3]. This is, of course, expected due to the following fact.

For $\alpha = \beta = \lambda$, using the transformation $\psi \to \psi e^{i\lambda t}$, the CGL equation can be written as [3]

$$\frac{\partial \psi}{\partial t} = (1 + i\lambda)(\psi + \nabla^2 \psi - |\psi|^2 \psi). \tag{2.17}$$

Further, writing $\psi = \psi_1 + i\psi_2$, Eq.(2.17) can be written for the time evolutions of ψ_1 and ψ_2 as

$$\frac{\partial \psi_1}{\partial t} = \psi_1 + \nabla^2 \psi_1 - |\psi|^2 \psi_1 - \lambda(\psi_2 + \nabla^2 \psi_2 - |\psi|^2 \psi_2) \tag{2.18}$$

and

$$\frac{\partial \psi_2}{\partial t} = \psi_2 + \nabla^2 \psi_2 - |\psi|^2 \psi_2 + \lambda(\psi_1 + \nabla^2 \psi_1 - |\psi|^2 \psi_1). \tag{2.19}$$

It is now quite clear that for the transformation $\lambda \to -\lambda$, merely ψ_1 changes to ψ_2 and vice versa. Thus we expect the pattern and dynamics to be same under change of sign for λ.

To learn about the growth exponent z, in Fig.2.13 we show the results for $\ell(t)$ for $\lambda = 0, 1, -1$ on a double-log scale. All the data sets are reasonably consistent with a power-law behavior. The dashed line there corresponds to $t^{1/2}$ growth which however is not perfectly parallel to the numerical data, particularly for $\lambda = 0$, i.e., the RGL equation. This discrepancy can be due to the presence of some initial length or time dependent correction to the exponent or the logarithmic correction in $d = 2$ that is mentioned in the Introductory section. We will check this subsequently.

Before moving into that, we take a relook at the length scale data for $\alpha \neq \beta$, in Fig.2.12. It is observed that there is a strange maximum at small t, for this case. We have previously mentioned that there is no scaling in the structure in case of spiral patterns. This maximum is due to that, as explained below.

In Fig.2.14, we take a look at the correlation functions for this case, viz., $\alpha = 1, \beta = 0$, as a function of r. Data from three different times are shown. It is seen that data for $t = 50$ decay slower than that for $t = 10$, as expected for normal phase ordering dynamics, say with vortex pattern. However, interestingly, data for $t = 1000$ falls faster than that for $t = 50$ and develops a minimum below zero [14]. This, of course, explains the maximum in Fig.2.12.

In view of the above, we also calculated $\ell(t)$ from Eq.(2.15)(see Fig.2.15). This calculation does not provide much additional information, for $\alpha = \beta$ will be however useful in the next chapter where we present quantitative results for $\alpha \neq \beta$.

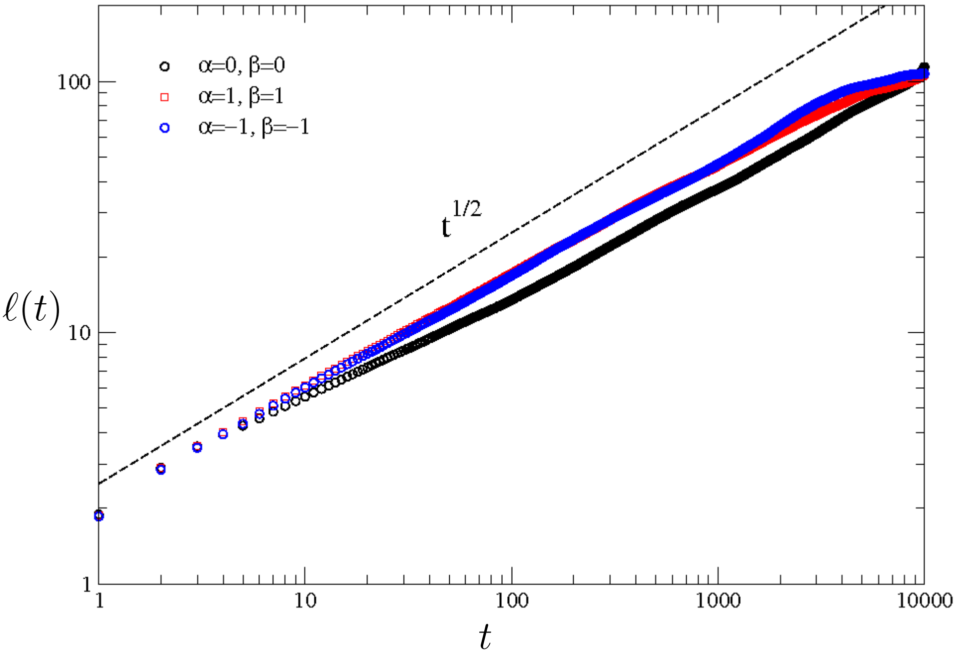

Figure 2.13: Same as Fig.2.12 but on a double double-log scale and data for $\alpha = 1, \beta = 0$ are excluded.

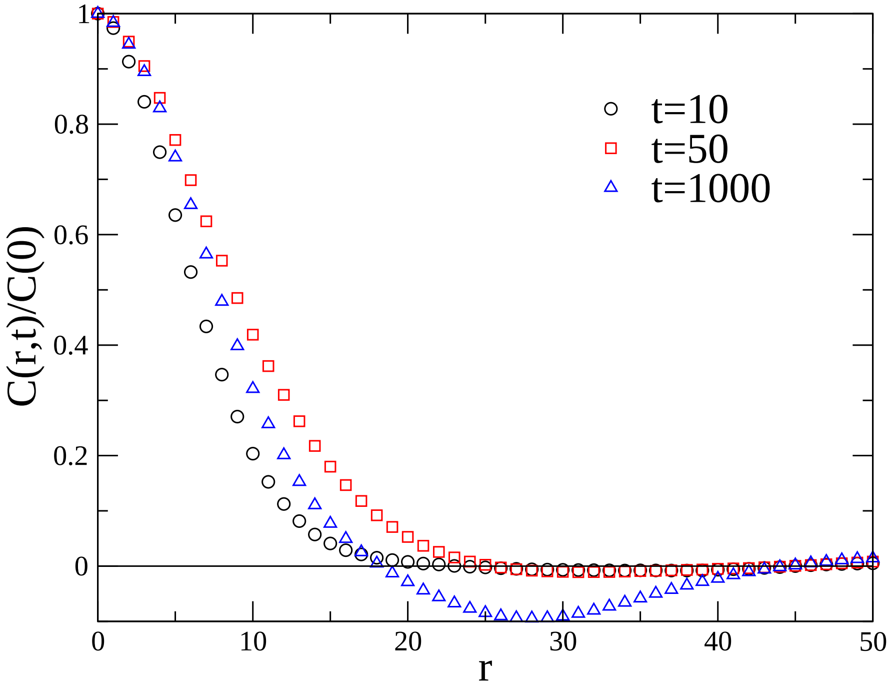

Figure 2.14: Plots of $C(r,t)$ vs r for $\alpha = 1, \beta = 0$. Data from three different times are shown.

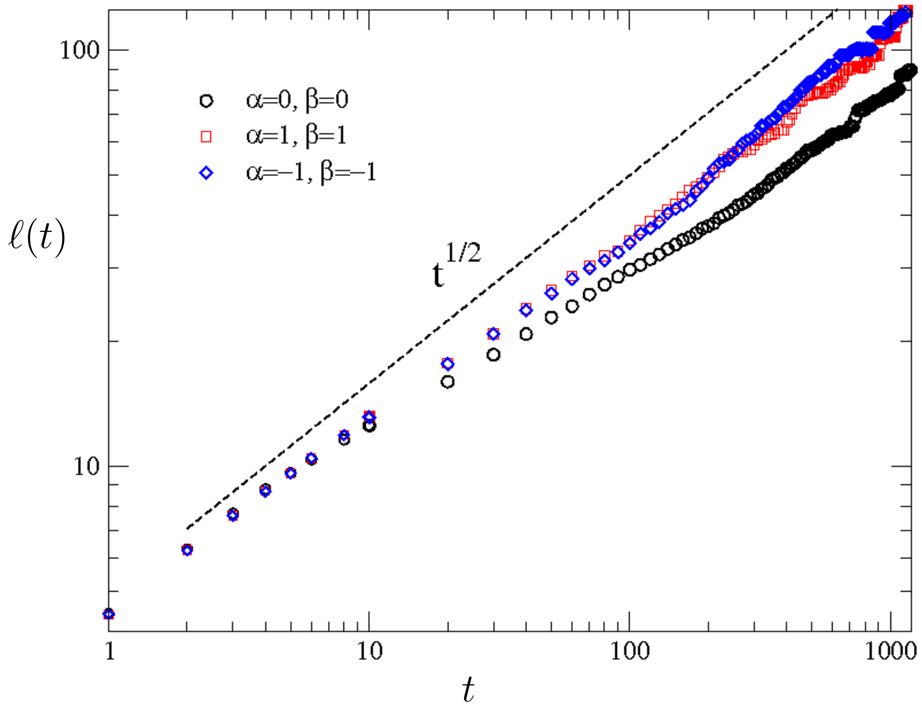

Figure 2.15: Plots of $\ell(t)$ vs t for $\alpha = \beta = -1, 0, 1$. As opposed to Fig.2.13, here $\ell(t)$ was obtained directly by calculating number of defects in the system at different instants.

Because of the mismatch of the numerical data with $t^{1/2}$ behavior in Figs.2.13 and 2.15, particularly for $\lambda = 0$, we present the instantaneous exponent $1/z_i$, calculated via Eq.(2.16), in Fig.2.16, as a function of $1/\ell(t)$. It is seen that in all the cases the numerical data have tendency to converge towards $z = 2$, in the limit $\ell \to \infty$. Being even on the conservative side, it can at least be concluded from this figure that the exponent z is reasonably close to 2 in all the cases. For further understanding of dependence of z on λ, in Fig.2.17 we show $\ell(t)$ vs t for more

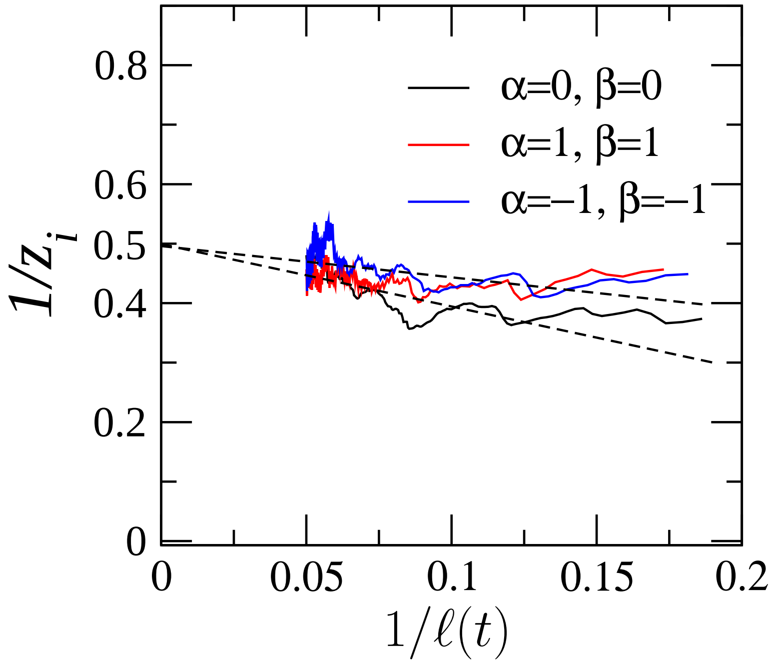

Figure 2.16: Plots of instantaneous growth exponent as a function of $1/\ell(t)$, for the data in Fig.2.13. The solid straight lines are guides to the eyes.

values of λ, on a double-log scale. It appears that with the increase of λ, the data become more parallel to $t^{1/2}$. This is an interesting fact and needs appropriate theoretical attention to understand. Here we note that the deviation of data, for $\lambda = 0$, from $t^{1/2}$ behavior could well be due to the logarithmic correction mentioned earlier. But to understand why this correction disappears for higher values of λ, one needs further studies.

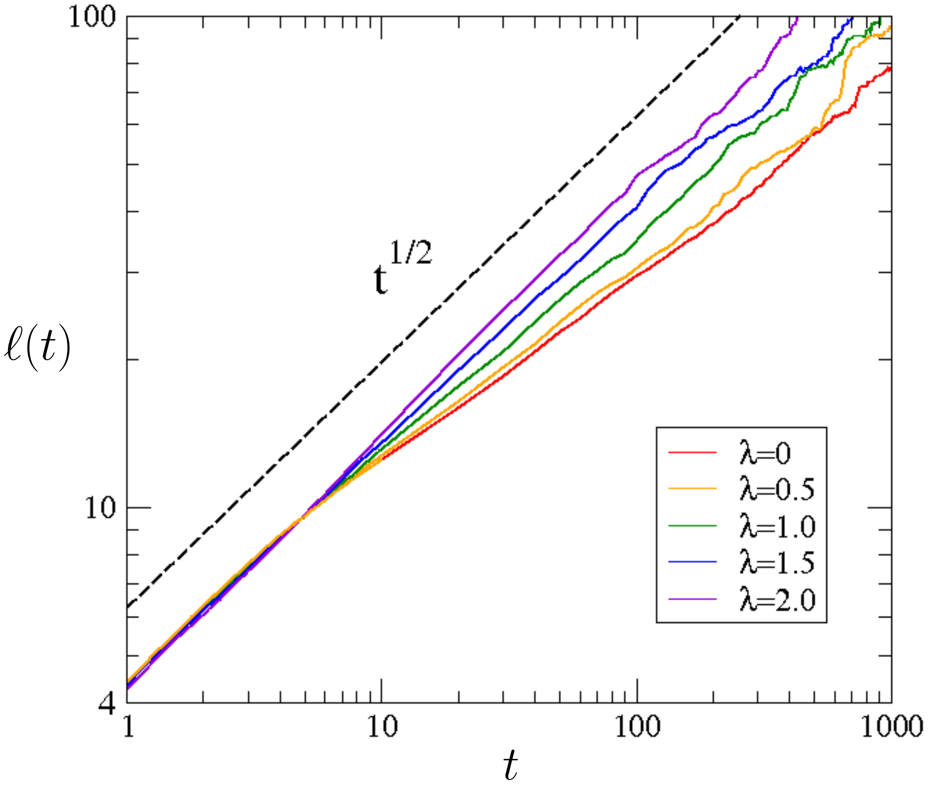

Figure 2.17: Plots of $\ell(t)$ vs t for multiple values of λ as indicated. A double log scale is used. The $t^{1/2}$ behavior is also indicated by the dashed line.

2.3.2 d=3

In this subsection, we present results from the solutions of the CGL equations in $d = 3$, for simple cubic lattice. In Fig.2.18 we show the snapshots for $\alpha = \beta = 0$ (a), 1 (b) and -1 (c). All the snapshots are from the same time. For the sake of clarity, we did not show the constant phase lines here. What is seen in these pictures are the vortex lines. As already mentioned, point defects at different planes meet to form these lines. Recall that the dimensionality of a defect [4] in d dimensions for n-component order parameter is $d-n$. Considering that we are working with 2-component order parameter in 3 space dimensions, we indeed expect such line defects.

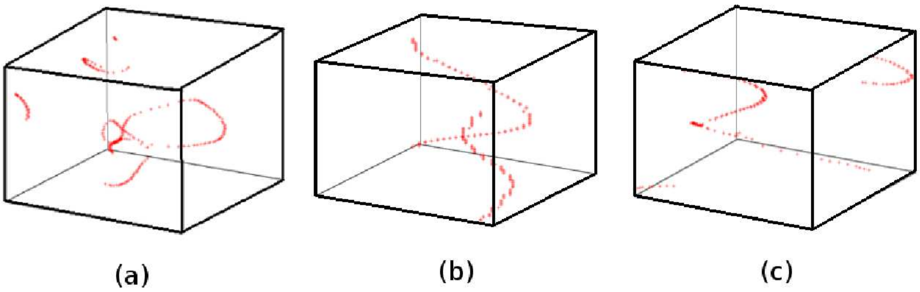

Figure 2.18: Snapshots from the evolutions of CGL equation in $d = 3$. Pictures are shown from one particular time for the combinations $\alpha = \beta = 0, 1, -1$. For the sake of clarity, only the defect cores are shown.

An important observation from Fig.2.18 is the following. While the defect density in (b) and (c) look similar, in (a) it is relatively higher. This is consistent with our observation in $d = 2$ that for $\lambda \neq 0$, the dynamics is faster than $\lambda = 0$, i.e., the RGL equation. Also, similar defect density in (b) and (c) reconfirm that dynamics for $\alpha = \beta = \pm\lambda$ are equivalent.

In Fig.2.19, we present the plots for $\ell(t)$ vs t for $\lambda = 0, -1$ and 1. Again, it is seen that data for $\lambda \neq 0$ are more consistent with the $t^{1/2}$ behavior. This, of course, raises question if our earlier conclusion about the logarithmic correction in $d = 2$ is correct!

2.4 Conclusion

In this chapter, we have presented results from the Euler discretized solutions of the CGL equation, in both d=2 and 3, using square and simple cubic lattices respectively.

In d=2, the single spiral solution was verified for different combinations of α and β. It appears that even for multi-spiral morphology, such solutions describe the system rather well, except for the shock regions where two spirals meet.

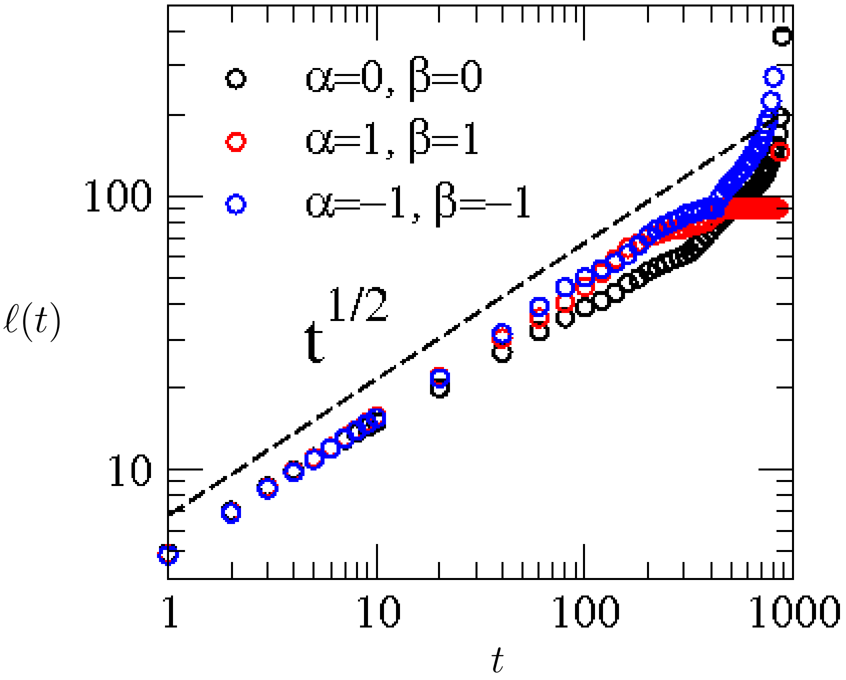

Figure 2.19: Plots of $\ell(t)$ vs t for 3-d CGL equations with $\alpha = \beta = -1, 0, 1$. A double-log scale is used. All data were obtained from the number of defects.

In both d=2 and 3, we have characterized the multi-defect pattern and dynamics of CGL equation for $\alpha = \beta = \lambda$. The $\lambda = 0$ case corresponds to the RGL equation. It is shown that, even for nonzero values of λ, the pattern is very similar to the RGL where vortex defects characterize the pattern formation. Further, for $\alpha = \beta$, in general, the characteristic length ℓ increases in a power-law fashion, with exponent very close to $z = 2$. We however, observed that, for $|\lambda| > 0$, the effective exponent is higher than the RGL.

Bibliography

[1] M. C. Cross and P. C. Hohenberg, Rev. Mod. Phys. **65**, 851 (1993).

[2] H. Chate and P. Manneville, Physica A **224**, 348 (1996).

[3] I. S. Anderson and L. Kramer, Rev.Mod. Phys., **74**, 1 (2002).

[4] A.J. Bray, Adv. Phys., **51**, 481 (2002).

[5] *Kinetics of Phase Transitions*, edited by S. Puri and V. Wadhawan (CRC Press, Boca Raton, FL, 2009).

[6] A. Onuki, *Phase Transition Dynamics*, (Cambridge University Press, Cambridge, UK, 2002).

[7] M. Plischke, B. Bergersen *Equilibrium Statistical Physics* (World Scientific, 2006).

[8] A.C. Newell, *Solutions in Mathematics and Physics*, CBMS Lect. Ser., Vol.**48** (SIAM Press, Philadelphia) 1983.

[9] P.S. Hagan, SIAM (Soc. Ind. Appl. Math) J. Appl. Math. **42**, 762 (1982).

[10] *Chemical Waves and Patterns*, edited by R. Kaperal and K. Showalter (Kluwer Academic, Dordrecht, 1993).

[11] A.J. Bray and S. Puri, Phys. Rev. Lett., **67**, 2670 (1991).

[12] H. Toyoki, Phys. Rev. B, **45**, 1965 (1992).

[13] I. S. Gradshteyn and I. M. Ryzhik, in *Table of Integrals, Series and Products*, edited by A. Jeffrey (Academic, London, 1994).

[14] S. K. Das, S. Puri and M. C. Cross, Phys. Rev. E, **64**, 046206 (2001).

[15] S. Puri, S. K. Das and M. C. Cross, *Phys. Rev. E* **64**, 056140 (2001).

[16] S. K. Das and S. Puri, Phys. Rev. E **65**, 046123 (2002).

[17] D. A. Huse, Phys. Rev. B **34**, 7845 (1986).

[18] S. K. Das, Phys. Rev. E **87**, 012135 (2013).

Chapter 3

Effect of Disorder in the Multi-Spiral Dynamics of Complex Ginzburg-Landau Equation

3.1 Introduction

In phase ordering dynamics, there has been much recent interest about the effect of disorder [1–8]. Significant understanding has been obtained in simple situations like random field and random bond Ising models. There it has been observed that introduction of disorder essentially slows down the rate of growth or ordering of the system. This happens due to creation of local energy barriers.

Such studies, however, are confined to systems with scaler order parameter, in the theoretical literature. Only recently [9, 10] the case of vector order parameter was considered in the context of complex Ginzburg-Landau (CGL) equation [11–13]

$$\frac{\partial \psi}{\partial t} = \psi + (1 + i\alpha)\nabla^2 \psi - (1 + i\beta)|\psi|^2 \psi, \tag{3.1}$$

where ψ is a space ($\vec{r}$) and time (t) dependent complex ($\rho e^{i\gamma}$) order parameter and α, β are real parameters. In this study [9, 10], α was set to zero and disorder was introduced in β. Note that, for $\alpha \neq \beta$ and for uniform values of these parameters throughout the whole system, CGL equation provide frozen spiral dynamics [12, 14–16]. In this study [9, 10], with disorder in β, it was, however, observed that this frozen dynamics is unlocked. Noting that in the context of Belouzov-Zhabotanski (BZ) reaction [17], β may correspond to the concentration of catalyst which is not really constant over space, the introduction of disorder is certainly physically meaningful. Further meaning can be added to it by noting the fact that in the BZ reaction one observes microscopically big spirals as opposed to the frozen states with very small spirals for constant values of α and β in the CGL equation. With the same reasoning, we feel, it is also important to investigate the effects of disorder in α. This chapter is devoted to that.

In this context, it is worth mentioning that there have been significant recent activities [9, 10, 18–22] in understanding or learning mechanisms to unlock statistical freezing in the CGL or similar equations. Here note that CGL equation can also be written as [13]

$$\frac{\partial \psi}{\partial t} = (1 + i\mu)\psi + (1 + i\alpha)\nabla^2\psi - (1 + i\beta)|\psi|^2\psi. \tag{3.2}$$

However, under a rotating frame transformation [13] $\psi \to \psi e^{i\mu t}$, Eq.(3.2) is equivalent to Eq.(3.1). In another recent study [18, 19], the freezing was unlocked by introducing space gradient in the value of the real parameter μ. This space variation in μ allowed formation of spirals with different frequencies. It was observed that spirals with higher frequencies grew at the cost of the ones with smaller frequencies, providing an all time coarsening dynamics. In the study with quenched randomness in β, however, it was shown that the mechanism of higher frequency spirals killing the smaller frequency ones is not true.

In another study [20], it was demonstrated that if a reaction-diffusion system, with two components and exhibiting frozen dynamics, is coupled to a slowly varying third component, the freezing can be unlocked.

We are interested in the unlocking of frozen dynamics in the CGL equation by invoking disorder in α and β. As already mentioned, this is our objective in this chapter rest of which is organized as follows. Having described the method in details in the previous chapter, we will straightaway present the results in Section 3.2. Note here that except for the last figure we will work only in $d = 2$. Finally, the chapter will be closed with a brief summary of results in Section 3.3.

3.2 Results

In Fig.3.1, we show the evolution snapshots from the solutions of the CGL equation on a 2-d square lattice of linear dimension $L = 256$, with Euler discretization mesh sizes $\Delta x = 1$ and $\Delta t = 0.01$. Throughout this chapter, we will use these values of Δx and Δt. For this picture, we have used $\alpha = 0, \beta = 1$. Here, in addition to showing the constant phase lines (with two different values of γ), we have also shaded the region [13, 23] where the amplitude ρ is larger than $\sqrt{1 - q^2}$. It appears that in prominent spiral regions, ρ is less than $\sqrt{1 - q^2}$ and shades appear mainly in the shock regions [12, 13], i.e., places where two spirals collide.

Similar snapshots are presented in Fig.3.2. This time we have set the parameters to $\alpha = 1$ and $\beta = 0$. Here also it is quite clear that in the shock regions ρ assumes value higher than $\sqrt{1 - q^2}$. In both the figures, viz., Figs.3.1 and 3.2, the values of α and β are uniform throught the system.

From both Fig.3.1 and Fig.3.2, it is quite evident that the dynamics

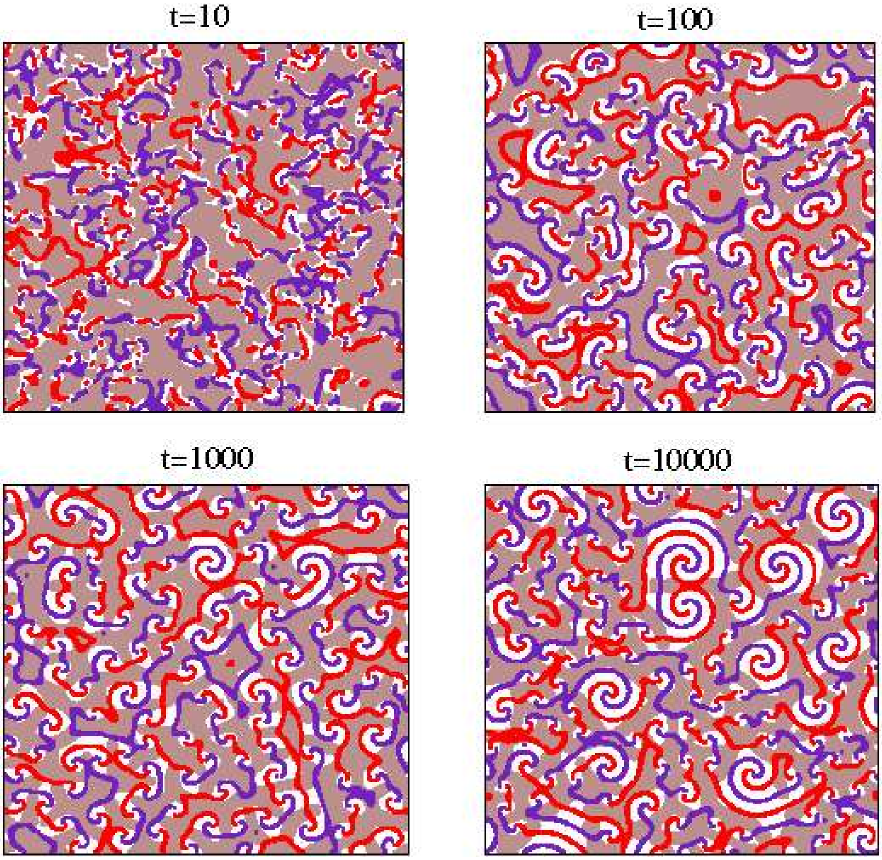

Figure 3.1: Snapshots from four different times during the evolution of the CGL equation with $\alpha = 0, \beta = 1; L = 256$, starting from random initial configuration using periodic boundary conditions. The color coding is same as Fig.2.1. The values of Δx and Δt were set to 1 and 0.01, respectively.

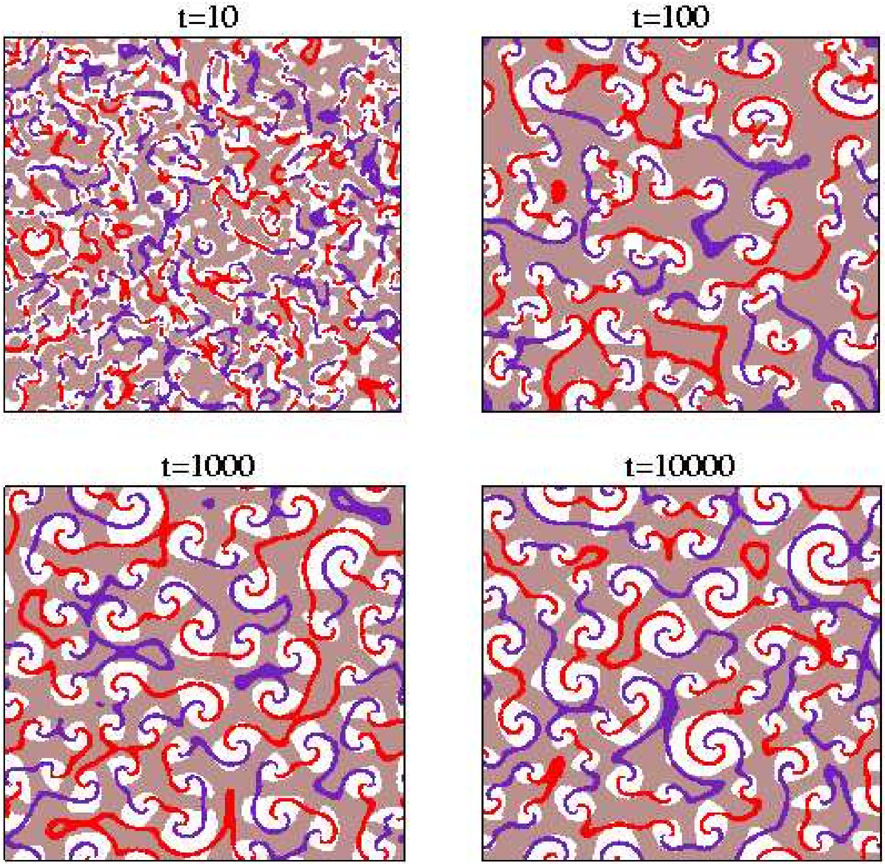

Figure 3.2: Same as Fig.3.1 but with the parameters $\alpha = 1, \beta = 0$.

gets frozen at later time, as already pointed out in the previous chapter. This is quantitatively demonstrated in Fig.3.3. In this figure we have plotted the average defect size $\ell(t)$ as a function of t. In addition to the cases $\alpha = 0, \beta = 1$ and $\alpha = 1, \beta = 0$, we have also included data from $\alpha = \beta = 0$, i.e., the real Ginzburg-Landau (RGL) equation [24], for the sake of comparison. In all the cases, $\ell(t)$ was calculated directly by counting the number of defects $N(t)$ at time t. It is clearly seen that for $\alpha \neq \beta$ cases, beyond a certain time ($\sim 10^2$), $\ell(t)$ ceases to grow.

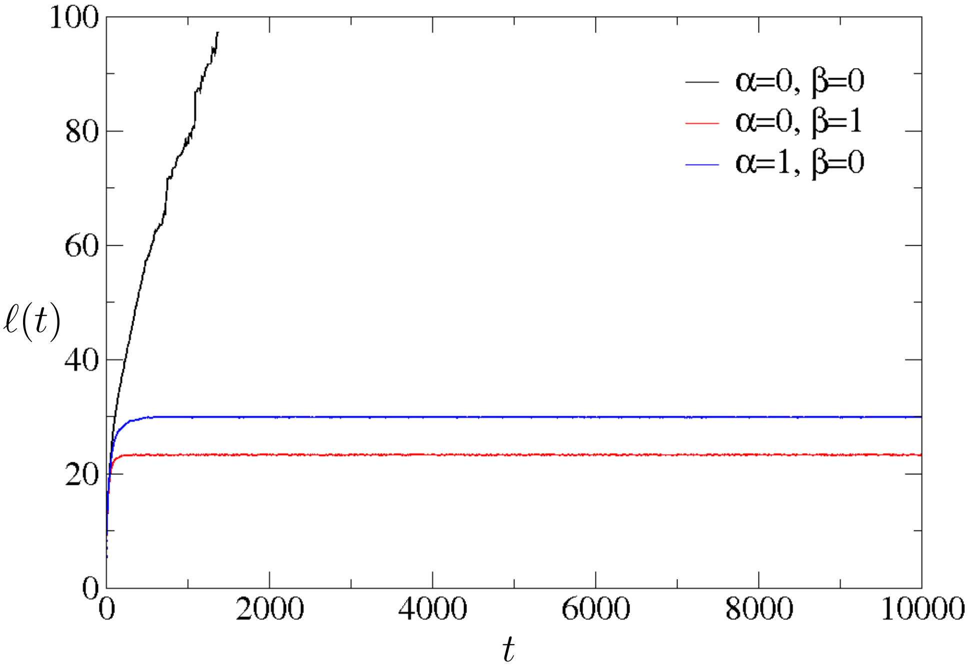

Figure 3.3: Plots of $\ell(t)$ vs t for three different combinations of α and β, as indicated.

Next we introduce disorder in α and β as

$$\alpha(x, y) \in [\alpha_0 \pm \delta\alpha] \tag{3.3}$$

and

$$\beta(x, y) \in [\beta_0 \pm \delta\beta], \tag{3.4}$$

where $\delta\alpha$ and $\delta\beta$ are uniformly distributed random numbers around the mean values α_0 and β_0, respectively. It will also be interesting to use random numbers from other distributions, e.g., Gaussian. But we do not expect any qualitative difference in results by doing so. In the rest of the chapter, we will refer to the values $\alpha_0, \beta_0, \delta\alpha$ and $\delta\beta$.

In Fig.3.4, we show the first snapshots with disorder. Here the parameter values are $\alpha_0 = 0, \delta\alpha = 0, \beta_0 = 1$ and $\delta\beta = 0.25$. Again, as earlier, two constant phase values are used. In this figure also shaded region corresponds to $\rho > \sqrt{1 - q^2}$ with q being the value corresponding to α_0 and β_0. It is clearly seen that the system is not trapped, rather it is continuously coarsening. Here also the shades appear along the shocks. Considering that q was calculated from the central values of α and β, this already says that spirals with only fixed values of q and ω exist, related to α_0 and β_0. The remark on q can be justified from the snapshots from where it is obvious that the gradient of phase along the radial directions

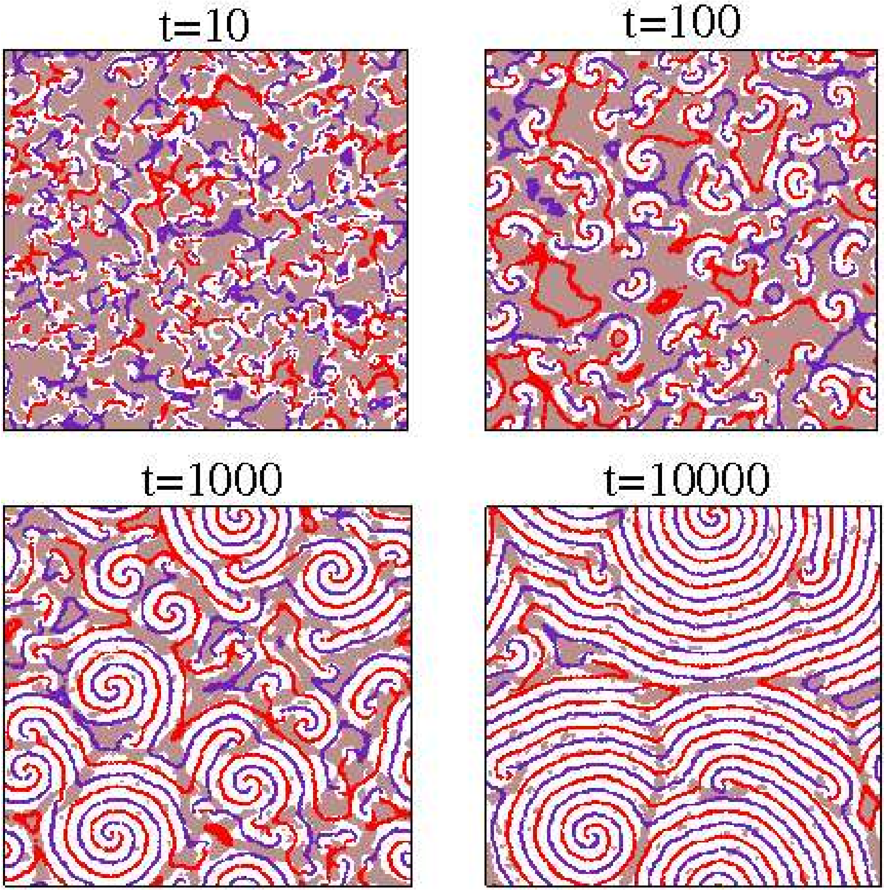

Figure 3.4: Same as Fig.3.1 but with introduction of spatial disorder in the value of β with the strength of disorder $\delta\beta = 0.25$.

for all spirals is same, at most with minor fluctuations.

In Fig.3.5 we present snapshots from four different times for the parameter values $\alpha_0 = 0, \delta\alpha = 0.25, \beta_0 = 1$ and $\delta\beta = 0$. The trend is qualitatively similar to the case in Fig.3.4. Essentially, there is no dynamical freezing in the system. In this case, the picture is even more clear that there exist defects corresponding to the central values of α and β, i.e., α_0 and β_0.

The last two figures nicely demonstrated that disorder in both α and β are capable of unlocking the frozen dynamics in the CGL equation. However, in both these cases we have used $\alpha_0 = 0$ and $\beta_0 = 1$. Next we examine a case with nonzero value of α_0.

In Fig.3.6 we present evolution snapshots for $\alpha_o = 1, \delta\alpha = 0.25, \beta_0 = 0$ and $\delta\beta = 0.0$. While there is some qualitative similarity of these results with the one in last two figures, in this case, the process of unlocking, if at all, is rather slow. Only at $t = 10000$, one big size spiral is emerging.

In Fig.3.7 we have shown the snapshots from same values of α_0 and β_0 as in Fig.3.6, but this time we have introduced disorder in β, i.e., the snapshots correspond to $\alpha_0 = 1, \delta\alpha = 0, \beta_0 = 0, \delta\beta = 0.25$. In this case, again, the effect is rather robust showing very fast growth of spirals. Another important observation here is that, even though the shades are mainly confined to the shock regions, they appear within the spirals also. But the appearance of shades inside the spirals has some random character. Perhaps because of this random character, the value

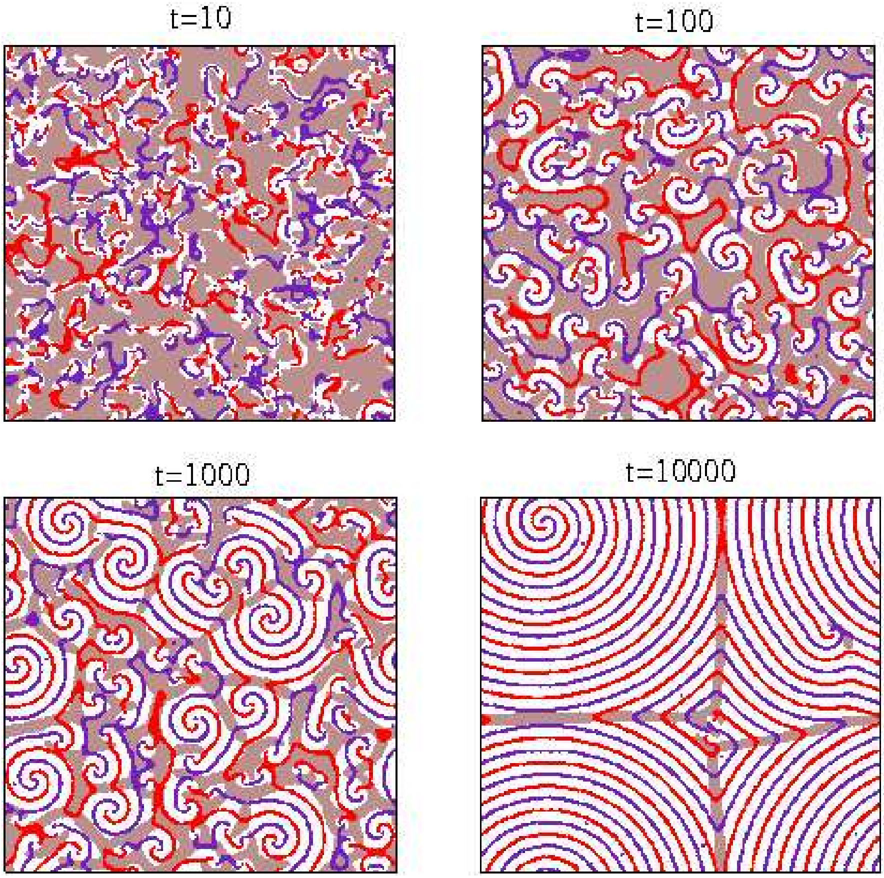

Figure 3.5: Same as Fig.3.1 but with introduction of spatial disorder in the value of α with the strength of disorder 0.25.

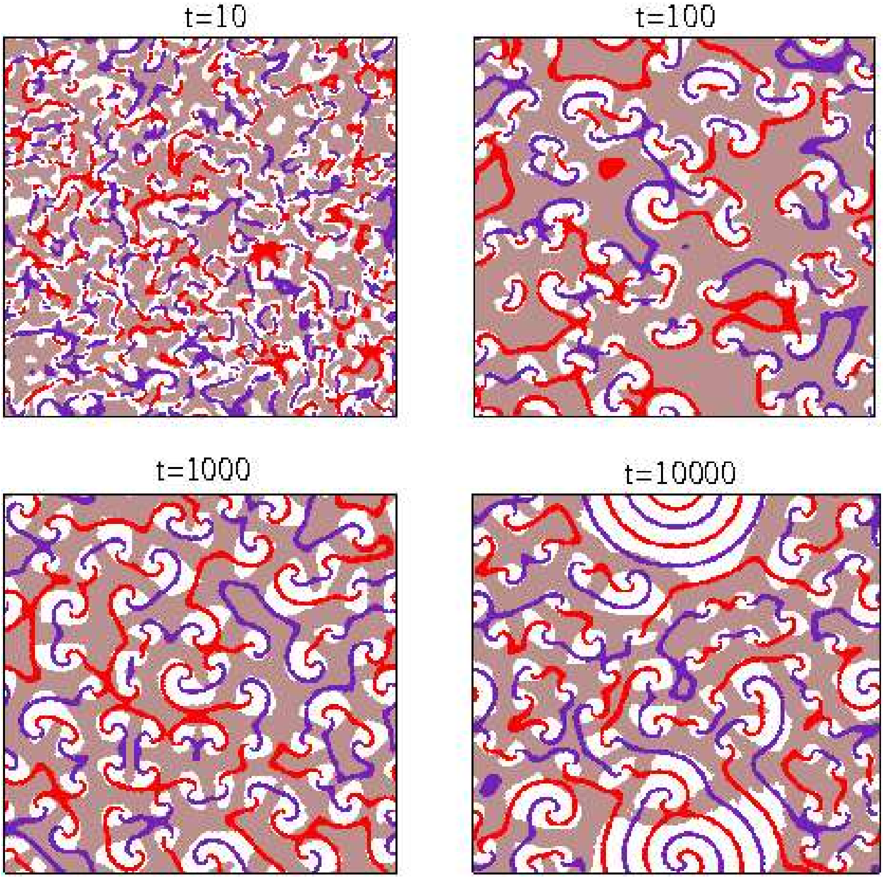

Figure 3.6: Same as Fig.3.2 but with introduction of spatial disorder in the value of α with the strength of disorder 0.25.

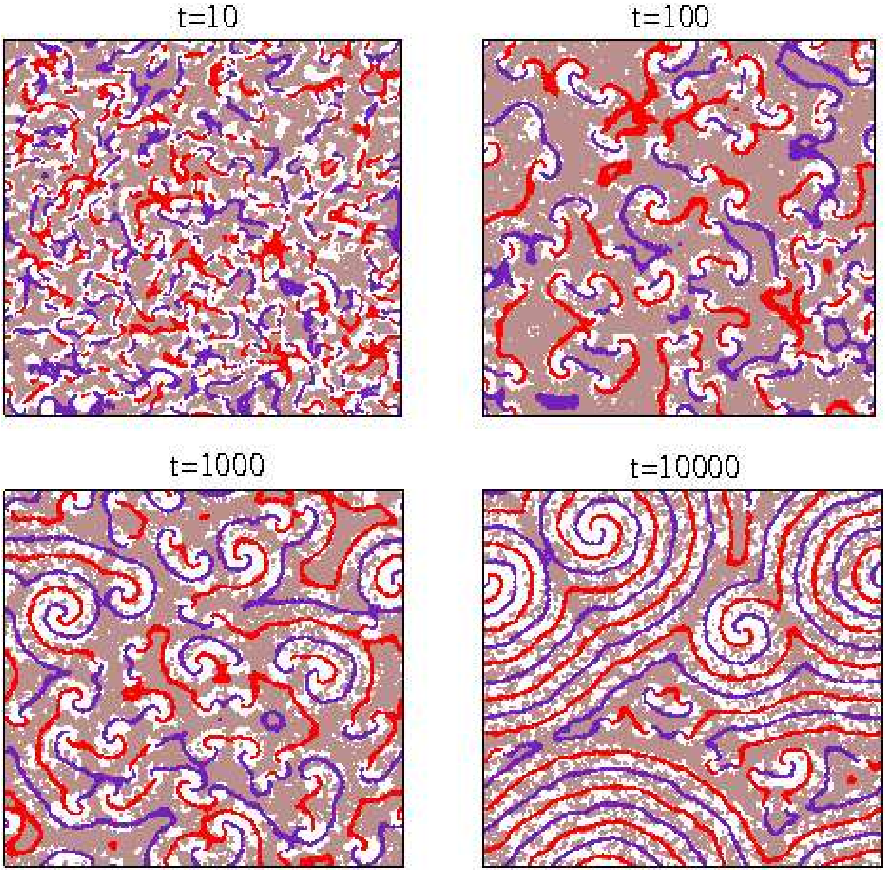

Figure 3.7: Same as Fig.3.2 but with introduction of spatial disorder in the value of β with the strength of disorder 0.25.

of q, i.e., the phase gradient along the radial direction does not exhibit any systematic change. Having drawn only qualitative conclusions, about the effect of disorder, from the snapshots, next we present quantitative results.

In Fig.3.8 we plot $\ell(t)$ as a function of t. Three sets of parameter values are included, as mentioned on the figure. As already discussed, for $\alpha_0 = 0, \beta_0 = 1, \delta\alpha = 0$ and $\delta\beta = 0$, we have frozen dynamics. But for disorder in α or β, both are showing nice increase in the average size of the spirals over the whole time range studied, confirming that disorder in both α and β, are independently capable of getting rid of the otherwise frozen dynamics.

In Fig.3.9 we show similar plots for the cases $\alpha_0 = 1$, $\beta_0 = 0$ and related disorders. Here it is seen that disorder in β is helping the system grow but disorder in α within this time window have not yet unlocked the freezing. In the latter case, even though the last snapshot in Fig.3.6 showed the appearance of a large spiral, the total number of spirals in the system did not decrease yet. From direct observation of the dynamics with disorder what we have learnt is the following. At intermediate time some big spirals push the smaller ones to one region. During this period practically no annihilation occurs. Only at much late time (this depends upon the parameters), when these small spirals are significantly nearby, very rapid annihilation occurs, providing a fast growth of length when calculated from the number of spirals $N(t)$. Note that forcing these small

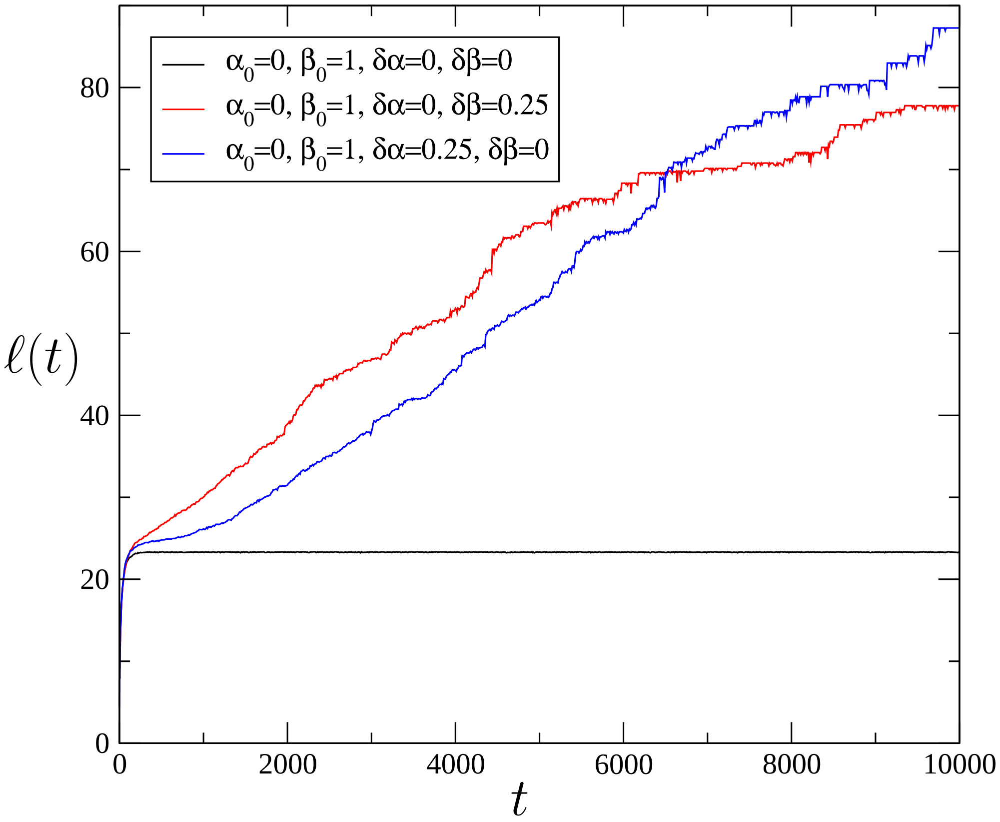

Figure 3.8: Plots of $\ell(t)$ vs t for three cases, viz., $\alpha_0 = 0, \beta_0 = 1, \delta\alpha = 0, \delta\beta = 0; \alpha_0 = 0, \beta_0 = 1, \delta\alpha = 0.25, \delta\beta = 0$ and $\alpha_0 = 0, \beta_0 = 1, \delta\alpha = 0.0, \delta\beta = 0.25$. A linear scale is used. In all the cases the data were obtained from the number of defects.

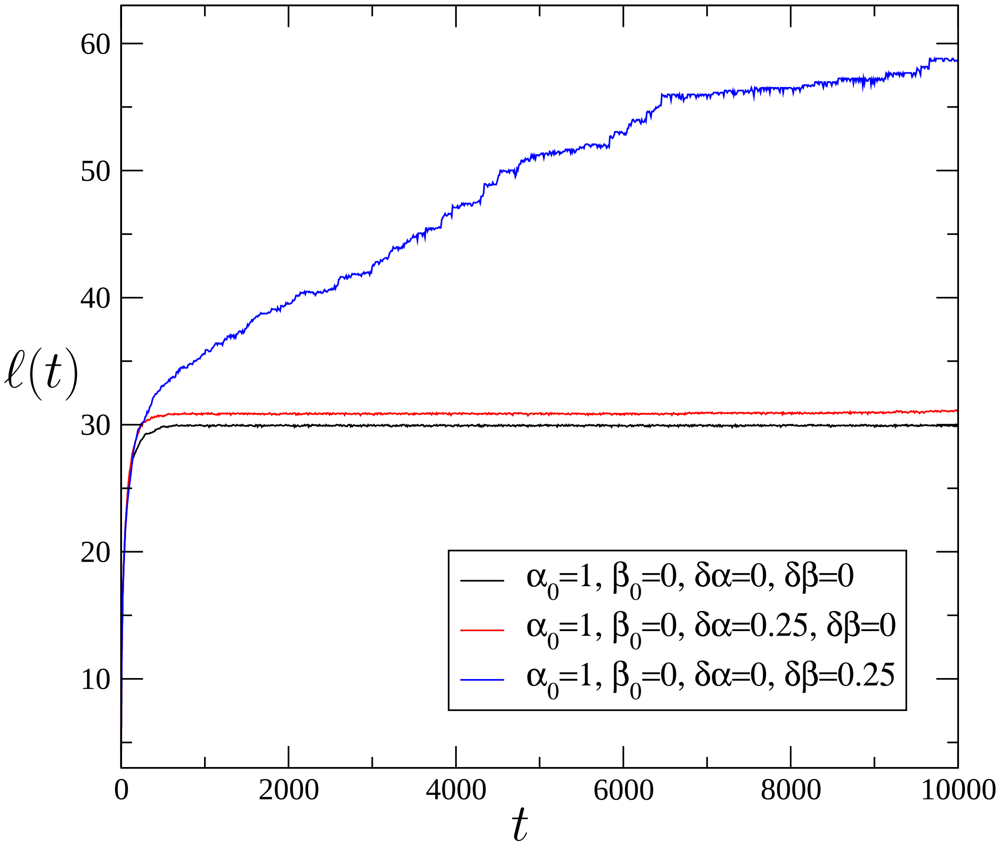

Figure 3.9: Similar to Fig.3.8, but with $\alpha_0 = 1, \beta_0 = 0$ and various combinations of disorder.

spirals to collide with each other may require significant time depending upon the height of the repulsive barrier which, in turn, depends upon the values of α and β. A knowledge about this interaction barrier, as a function of α and β, to the best of our knowledge, is still lacking in the literature. Once this barrier is overcome, the spirals can spontaneously approach and annihilate each other to make the growth possible. Further, what makes the big spirals to push the smaller ones due to the introduction of disorder is a nontrivial task to understand and certainly requires significant theoretical attention. Here we mention that these results are extremely counter intuitive consider the effects of disorder in Ising like systems reported in the literature [1–7].

Finally, in Fig.3.10 we present results from the solutions of the CGL equation in $d = 3$ for a simple cubic lattice. For the sake of brevity, we show only the plots of $\ell(t)$ vs t. In this figure we have included two sets of parameter values, each with $\alpha_0 = 1$ and $\beta_0 = 0$. For the case without any disorder, i.e., $\delta\alpha = 0$ and $\delta\beta = 0$, here also we observed freezing. However, it is seen that, for $\delta\alpha = 0.25, \delta\beta = 0$, the system continuously grows. For the computational demand to deal with $3 - d$ systems, we have confined our studies to these two sets of parameters only.

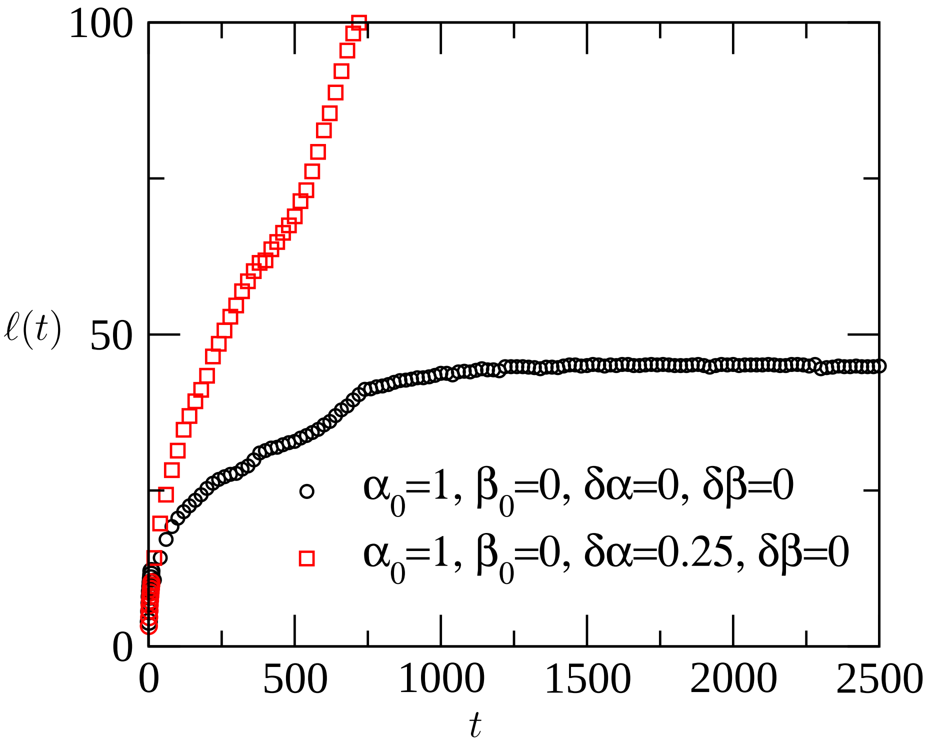

Figure 3.10: Plots of $\ell(t)$ vs t obtained from 3-d simulations of the CGL equations for $\alpha_0 = 1, \beta_0 = 0, \delta\alpha = 0, \delta\beta = 0$ and $\alpha_0 = 1, \beta_0 = 0, \delta\alpha = 0.25, \delta\beta = 0.0$. A linear scale is used. In all the cases the data were obtained from the number of defects.

3.3 Conclusion

In this chapter we have presented results for the pattern and dynamics in the complex Ginzburg-Landau equation [11–13] for $\alpha \neq \beta$. For all combinations it is observed that the patterns are characterized by spiral defects.

For constant values of α and β throughout the system, the dynamics gets locked, in a statistical sense, beyond a certain time and length that depend upon the values of α and β. Interestingly, randomness in the values of α and β is capable of unlocking the dynamics.

The reason behind such unlocking in the disordered cases we do not clearly understand and the phenomena is certainly counter-intuitive considering our lesson from other phase ordering systems, e.g., in random bond and random field Ising models [1–7], the effects of disorder is to slow down the growth.

A reason for the opposite effect in the present problem can possibly be understood in the following way. Note that the amplitude of the order parameter deviates from the single spiral solution, discussed in the previous chapter, in shock region. This might be a possible reason for the spiral-antispiral repulsive barrier. In fact, in a recent study [10], it was shown that if the amplitude in the shock region is artificially suppressed to the asymptotic ($r \to \infty$) value predicted by this single spiral solution, the spirals are again able to favorably interact with each other to come closer. Perhaps, the disorder also somehow modulates the value of amplitude to overcome this barrier. Nevertheless, we feel that more sophisticated studies are needed to understand this interesting phenomena.

Bibliography

[1] D. A. Huse and C. L. Henley, Phys. Rev. Lett. **54**, 2708 (1985).

[2] D. A. Huse and D. S. Fisher, Phys. Rev. B **38**, 373 (1988).

[3] S. Puri, D. Chowdhuey and N. Parekh, J. Phys. A : math. Gen. 24, L1087 (1998)

[4] J. P. Bonchaud, V. Dupuis, J. Hammann and E. Vinvent, Phys. Rev. B **65**, 024439 (2001).

[5] M. Henkel and M. Pleimling, Europhys. Lett. **76**, 561 (2006).

[6] C. Aron, C. Chamon L. F. Cugliandolo and M. Picco, J. Stat. Mech. P05016 (2008).

[7] F. Corberi, E. Lippiello, A. Mukherjee, S. Puri and M. Zannetti, J. Stat. Mech. P03016 (2011).

[8] V. Banerjee and S. Dattagupta, Physica A **224**, 226 (1996).

[9] S. K. Das, Europhys. Lett. **97**, 46006 (2012).

[10] S. K. Das, Phys. Rev. E **87**, 012135 (2013).

[11] M. C. Cross and P. C. Hohenberg, Rev. Mod. Phys. **65**, 851 (1993).

[12] H. Chate and P. Manneville, Physica A **224**, 348 (1996).

[13] I. S. Aranson and L. Kramer, Rev. Mod. phys. **74**, 1 (2002).

[14] S. K. Das, S. Puri and M. C. Cross, Phys. Rev. E **64**, 046206 (2001).

[15] S. Puri, S. K. Das and M. C. Cross, Phys. Rev. E **64**, 056140 (2001).

[16] S. K. Das and S. Puri, Phys. Rev. E **65**, 046123 (2002).

[17] *Chemical eaves and Patterns*, edited by R. Kapral and K. Showalter (Kluwer Academic, Dordrecht, 1993).

[18] M. Hendrey, E. Ott and T. M. Antonsen, Jr., Phys. Rev. Lett. **82**, 859 (1999).

[19] M. Hendrey, E. Ott and T. M. Antonsen, Jr., Phys. Rev. E **61**, 4943 (2000).

[20] I. Aranson, H. Levine and L. Tsimring, Phys. Rev. Lett. **76**, 1170 (1996).

[21] T. K. Shajahan, S. Sinha and R. Pandit, Phys. Rev. E **75**, 011929 (2007).

[22] W. Guo, C. Qiao, Z. Zhang, Q. Ouyang and H. Wang, Phys. Rev. E **81**, 056214 (2010).

[23] P. S. Hagan, SIAM (Soc. Ind. Appl. Math.) J. Appl. Math. **42**, 762 (1982).

[24] A. J. Bray, Adv. Phys. **51**, 481 (2002).

Appendix

1. At the end of the paragraph containing Eq.(1.5), we add "The first and third terms in the right hand side of Eq.(1.5) form $f(\lambda, \psi)$, the reaction term in a reaction-diffusion situation and the second term corresponds to diffusion. For $\alpha = \beta = 0$, they come directly from the coarse-graining of the Ising model. In case of coupled oscillator equations, α and β simply are coupling constants. An educative phase diagram in the plane of these parameters are presented in Physica A **224**, 348 (1996). The diagram is rather complex. For $\alpha = 0$, we discuss it with respect to the variation in β. Within the range $0 \leq \beta \leq 1.397$, the spirals, the pattern the CGL equation exhibits, are linearly stable. For $1.397 < \beta \leq 1.82$, the spirals are linearly unstable to fluctuations and beyond that the spirals are globally unstable—essentially, one enters a chaotic regime. In this thesis we will deal with parameter values that provide stable pattern."

2. We add the following snapshot to Fig.3.6, in addition to the ones presented.

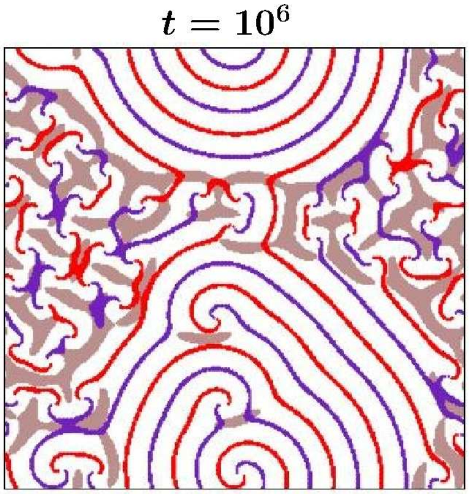

3. The y-axes in the Figs.2.15, 2.17, 3.3, 3.8, 3.9 should be scaled by a factor 1.1.